

Susceptibility-weighted Imaging: Technical Essentials and Clinical Neurologic Applications

Sven Haller, MD, MSc, • E. Mark Haacke, PhD • Majda M. Thurnher, MD • Frederik Barkhof, MD, PhD

From the CIRD Centre d'Imagerie Rive Droite, Geneva, Switzerland (S.H.); Faculty of Medicine of the University of Geneva, Geneva, Switzerland (S.H.); Department of Surgical Sciences, Division of Radiology, Uppsala University, Uppsala, Sweden (S.H.); CIMC Centre d'Imagerie Médicale de Cornavin, Geneva, Switzerland (S.H.) Departments of Neurology and Radiology, Wayne State University, Detroit, Mich (E.M.H.); Department of Biomedical Imaging and Image-guided Therapy, Medical University Vienna, Vienna, Austria (M.M.T.); Queen Square Institute of Neurology, University College London, London, England (F.B.); Centre for Medical Image Computing (CMIC), Institute of Healthcare Engineering, University College London, London, England (F.B.); and Department of Radiology and Nuclear Medicine, Amsterdam University Medical Centre, Amsterdam, the Netherlands (F.B.). Received July 14, 2020; revision requested September 8; revision received September 18; accepted November 16. Address correspondence to S.H. (e-mail: sven.haller@me.com).

Conflicts of interest are listed at the end of this article.

Radiology 2021; 299:3–26 • <https://doi.org/10.1148/radiol.2021203071> • Content codes: **NR** **MR**

Susceptibility-weighted imaging (SWI) evolved from simple two-dimensional T2*-weighted sequences to three-dimensional sequences with improved spatial resolution and enhanced susceptibility contrast. SWI is an MRI sequence sensitive to compounds that distort the local magnetic field (eg, calcium and iron), in which the phase information can differentiate. But the term *SWI* is colloquially used to denote high-spatial-resolution susceptibility-enhanced sequences across different MRI vendors and sequences even when phase information is not used. The imaging appearance of SWI and related sequences strongly depends on the acquisition technique. Initially, SWI and related sequences were mostly used to improve the depiction of findings already known from standard two-dimensional T2*-weighted neuroimaging: more microbleeds in patients who are aging or with dementia or mild brain trauma; increased conspicuity of superficial siderosis in Alzheimer disease and amyloid angiopathy; and iron deposition in neurodegenerative diseases or abnormal vascular structures, such as capillary telangiectasia. But SWI also helps to identify findings not visible on standard T2*-weighted images: the nigrosome 1 in Parkinson disease and dementia with Lewy bodies, the central vein and peripheral rim signs in multiple sclerosis, the peripheral rim sign in abscesses, arterial signal loss related to thrombus, asymmetrically prominent cortical veins in stroke, and intratumoral susceptibility signals in brain neoplasms.

©RSNA, 2021

Online supplemental material is available for this article.

Online SA-CME • See www.rsna.org/learning-center-ry

Learning Objectives:

After reading the article and taking the test, the reader will be able to:

- Describe how technical parameters of susceptibility-weighted imaging (SWI) and SWI-like sequences impact image appearance and consequently image interpretation
- Describe how imaging of the nigrosome 1 territory flanked by two hypointense linear bands, which resemble a swallow tail, contributes to the diagnosis of parkinsonian syndromes and dementia with Lewy bodies
- Identify additional imaging signs of SWI and SWI-like sequences in a variety of diseases

Accreditation and Designation Statement

The RSNA is accredited by the Accreditation Council for Continuing Medical Education (ACCME) to provide continuing medical education for physicians. The RSNA designates this journal-based SA-CME activity for a maximum of 1.0 AMA PRA Category 1 Credit®. Physicians should claim only the credit commensurate with the extent of their participation in the activity.

Disclosure Statement

The ACCME requires that the RSNA, as an accredited provider of CME, obtain signed disclosure statements from the authors, editors, and reviewers for this activity. For this journal-based CME activity, author disclosures are listed at the end of this article.

MRI offers a broad range of contrast mechanisms that exploit key tissue properties including water content (spin density), T1, T2, diffusion, T2*, and susceptibility. There is growing interest in T2*-weighted imaging and the underlying susceptibility effects in the form of both susceptibility-weighted imaging (SWI) (1,2) and quantitative susceptibility mapping (QSM) (3). The former has been available to clinicians for nearly 20 years, whereas the latter remains in a research mode after more than 10 years of development. Interpreting these different contrast mechanisms is not always straightforward and this is true with the subtleties associated with SWI.

SWI is the combination of a specific sequence and processing design developed to enhance the contrast in T2*-weighted images (1). Originally developed to look at deoxyhemoglobin in veins and cerebral microbleeds

(CMBs), its applications have widened considerably. SWI combines a high-spatial-resolution, ideally fully flow-compensated (to avoid vascular dephasing caused by flow effects), and three-dimensional gradient-echo sequence with a phase mask to highlight paramagnetic and/or diamagnetic substances.

Different MRI vendors have proposed various techniques with the same intention to provide high-spatial-resolution sequences that enhance the susceptibility contrast for clinical routine.

To avoid confusion or misunderstandings, our article will use the term *SWI* only for sequences that apply a specific filtering and phase multiplication (1) and the term *SWI-like* will be used as a generic term for all types of high-spatial-resolution susceptibility-enhanced heavily T2*-weighted sequences across all vendors.

Abbreviations

APS = atypical parkinsonian syndrome, CMB = cerebral microbleed, N1 = nigrosome 1, PD = Parkinson disease, QSM = quantitative susceptibility mapping, SWI = susceptibility-weighted imaging, TE = echo time

Summary

Susceptibility-weighted imaging is an increasingly important adjunct in diagnosing a variety of neurologic diseases and provides a powerful tool to depict and help characterize microbleeds, veins, and other sources of susceptibility.

Essentials

- The fundamental aspects of magnetic susceptibility are explained to facilitate proper interpretation of susceptibility-weighted imaging (SWI) including phase information.
- The term *SWI* is colloquially used to denote high-spatial-resolution susceptibility-enhanced sequences across different MRI vendors and sequences, although SWI postprocessing was not necessarily performed.
- SWI-derived phase information helps to discriminate blood products from calcification.
- SWI and related sequences improve the depiction of lesions and signs already known from standard T2*-weighted imaging including cerebral microbleeds, superficial siderosis, iron deposition, and vascular diseases.
- Findings specific to SWI and related sequences include visualization of the nigrosome 1, central vein and peripheral rim sign, arterial signal loss, asymmetrically prominent cortical veins, and intratumoral susceptibility signals.

Technical Considerations

Essential Technical Considerations of Gradient-echo Imaging

Conventional T2-weighted imaging typically uses spin-echo sequences that minimize susceptibility artifacts (even with fast implementations) because of repetitive refocusing of 180° pulses. However, T2*-weighted, SWI, or SWI-like sequences purposely enhance the effect of local field variations caused by tissue content such as blood products (ie, hemosiderin in CMB), iron content (often in the form of ferritin), calcium content, and deoxyhemoglobin in venous blood. These processes cause local variations in the magnetic field that lead to signal loss in the form of T2* (Fig 1).

Historically, susceptibility effects used a two-dimensional gradient-echo T2*-weighted sequence (4). Because of restrictions regarding the number of sections required and the intermediate repetition times used, whole-brain coverage used only a relatively short echo time (TE) composed of sensitization to T2* signal loss. These sequences also used a small flip angle, making the images spin-density weighted and making the cerebrospinal fluid high contrast relative to the surrounding tissues (5). The TEs around 20–25 msec at 1.5 T made only larger microbleeds visible because the visibility of CMBs depends on TE and spatial resolution. High-spatial-resolution three-dimensional gradient-echo sequences show much smaller CMBs, especially when longer TEs are used.

Spin dephasing in the presence of local variations in the magnetic field causes susceptibility-related signal loss and depends

on spatial resolution and orientation of the object of interest (6). With current choices of TEs, if an object such as a vein or microbleed is about one-quarter of the voxel volume it will have the best cancellation effect (7). To highlight vessels or CMBs that are 250–500 μm in diameter, a voxel with dimensions 0.5 (readout) × 0.5 (phase) × 2 (partition) mm³ will maximize signal loss at a reasonably short TE. For practical reasons, we do not recommend the use of voxel sizes larger than 0.5 × 1 × 2 mm³. For venous blood (with a susceptibility of roughly 450 ppb, oxygen saturation of 70%, and a hematocrit of 45%), maximum signal loss occurs with a TE of around 23 msec at 3.0 T (46 msec at 1.5 T, and 9.8 msec at 7.0 T). The loss in magnitude for smaller objects will be less. Thus, the object might not be conspicuous despite a susceptibility effect in the phase images. Instead, the signal loss for bigger vessels will only occur at the edges of the vessels, creating a dark-line artifact around the vessel (7). Practically, a minimum-intensity projection (often more than four or five sections) highlights the continuity of the veins.

Basic Underpinnings of SWI Postprocessing

The concept of filtering the phase to highlight paramagnetic structures was a key advancement in developing SWI (8,9) and eventually in the use of the nomenclature *SWI* (1). Whereas any gradient-echo sequence can be reconstructed to produce magnitude and phase images, the diagnostic information in phase data is often corrupted by the effects of air and/or tissue interfaces and phase aliasing. But after high pass filtering the phase data, interesting contrast becomes available. The modification of filtered phase images can create a mask that highlights either paramagnetic (eg, hemosiderin or deoxygenated blood) or diamagnetic substances (eg, calcium, white matter fibers) depending on their positive and negative phase shifts. The creation of SWI data involves multiplying the phase mask (normalized between 0 and 1) several times (4 is usually enough to highlight most vessels while maintaining good signal-to-noise ratio) with the magnitude image to obtain the desired contrast (1). To enhance the visibility of veins and other sources of susceptibility, SWI is often postprocessed by using a minimum-intensity projection over multiple sections depending on the section thickness (Fig E1 [online]).

From a technical perspective, the term *SWI* is a particular processing method implemented on scanners manufactured by Siemens, United, and Neusoft. Similar susceptibility-weighted sequences exist, such as susceptibility-weighted angiography, or SWAN, by GE Healthcare and SWI with phase enhancement, or SWIp, by Philips. Susceptibility-weighted angiography uses magnitude images only, whereas SWI with phase enhancement also uses a phase mask. There are subtle differences between the vendors' implementation of SWI-like sequences (10). Those vendors that use SWI in its original implementation use a phase mask to enhance the contrast. But those that use SWI-like weighted images such as susceptibility-weighted angiographic images or venous blood oxygen level-dependent images use the magnitude images from longer TEs. The former uses a weighted sum of longer TEs to keep the T2* dephasing effects but also enhances the signal-to-noise ratio, whereas the latter uses a single long echo from an echo-shifted approach by a steady-state free

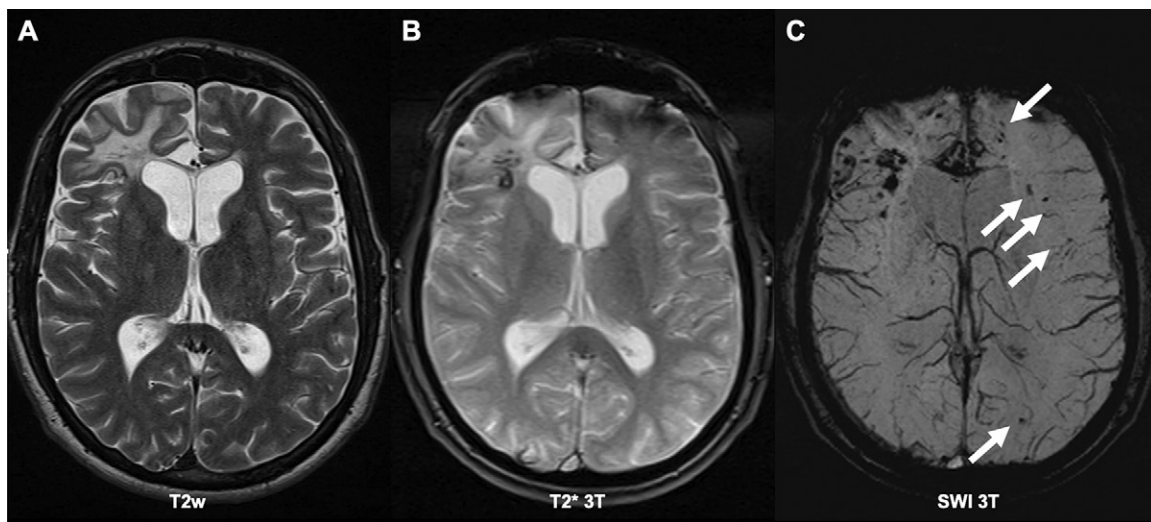


Figure 1: Axial MRI scans of multiple traumatic cerebral microbleeds in a patient with alcoholism and repetitive falls. A, A conventional spin-echo T2-weighted (T2w) image depicts the posttraumatic gliosis in the right frontal pole but shows no microbleeds. B, A conventional intermediate-echo T2*-weighted 3.0-T image depicts some evidence of hemosiderin and bleeding. C, Susceptibility-weighted imaging (SWI) findings show diffuse microbleeds and vascular damage in the frontal lobes (arrows) and show the veins because of their inherent deoxyhemoglobin content.

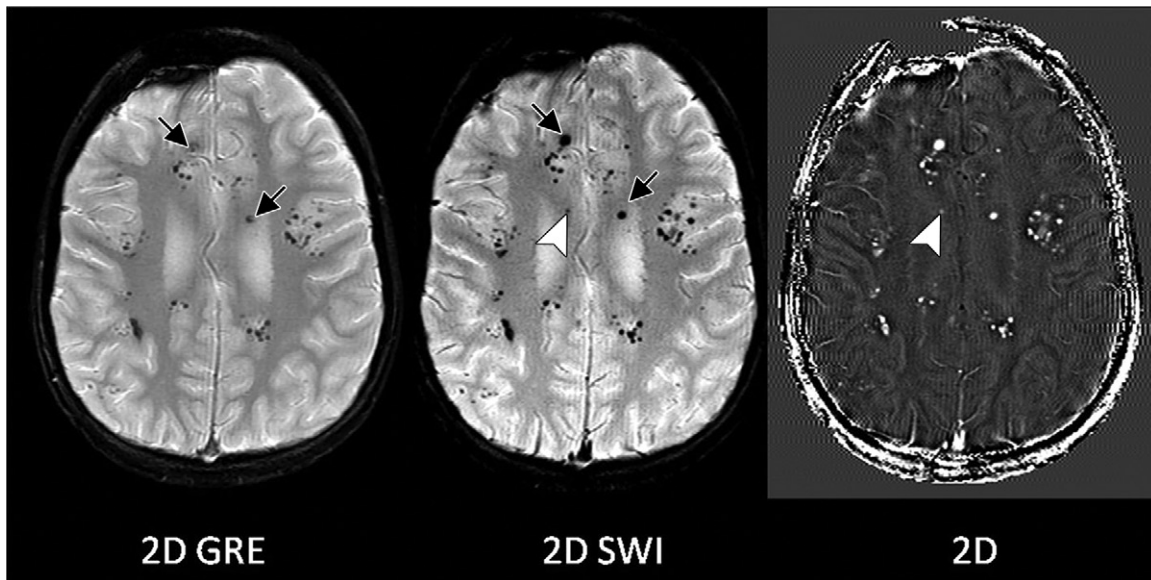


Figure 2: Images show the effect of the application of susceptibility-weighted imaging (SWI) scan processing on standard two-dimensional (2D) T2*-weighted gradient-echo (GRE) imaging (left). The resulting SWI contrast-enhanced image improves the detectability of microbleeds (middle) on the basis of the same data set. Microbleeds are better visible after SWI postprocessing (arrows); some can only be seen after SWI postprocessing (arrowheads). (Reprinted, with permission, from reference 57.)

precession imaging sequence. The main differences between these methods relate to the use of only T2* or a combination of T2* and phase. The use of only T2* has limited contrast compared with SWI but still does a good job at high fields because T2* effects are prevalent there with long echoes. The use of a combination of T2* and phase has poor phase behavior at the edge of the sinuses that exacerbates the loss of signal or bites out of the brain in the long-TE magnitude images, causing even more signal dropout in that territory.

SWI processing can be applied to two-dimensional gradient-echo sequences (Fig 2) and the usual three-dimensional sequences. It is also possible to apply post hoc SWI postprocessing

similar to the proposition by Haacke et al (1) to sequences from any MRI vendor, which do not routinely apply this postprocessing pipeline. For example, SWI postprocessing can be applied to data from the multiecho susceptibility-weighted angiography (GE Healthcare) sequence by using the phase information to improve the susceptibility contrast (Fig 3).

Phase Handedness and Geometry Dependence

Another key issue is how the vendors display the phase information. A left-handed system means the phase is positive going clockwise, whereas a right-handed system (the usual choice) means the phase is positive going counterclockwise (because

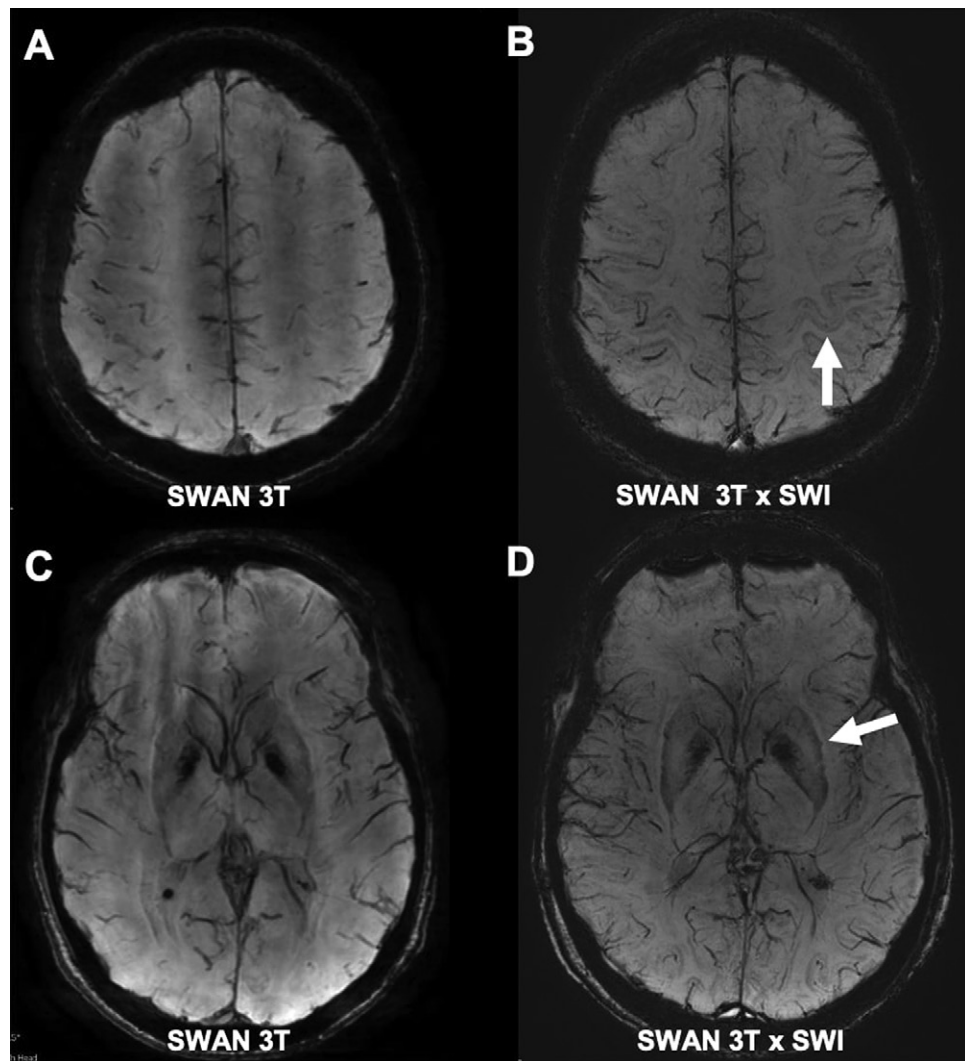


Figure 3: Appearance of veins and other structures with susceptibility in nonphase-processed versus phase-processed susceptibility-weighted imaging (SWI) data. A, C, A standard, multiecho, susceptibility-enhanced, susceptibility-weighted angiography (SWAN; GE Healthcare) sequence without SWI phase postprocessing. B, D, The post hoc application of SWI postprocessing to the exact same dataset changes the visual impression of the basal ganglia, cortical, and venous contrast (arrow).

that is the direction the fingers of your right hand will curl when you start with them straight and then make a fist). Vendors' sequence trade names are shown in Table 1. Depending on the use of left-handed versus right-handed systems, the image appearance changes (Fig 4).

There is no unique phase spatially outside an object. Both the phases inside and outside depend on geometry. For example, there is a dipole effect around each object (whether it is a CMB or a vein [paramagnetic] or calcium [diamagnetic]) that will change the phase as a function of the angle relative to the main field and position relative to the center of the object. By using these dipole effects, what is paramagnetic and what is diamagnetic can be better defined (Fig 5).

Microbleeds versus Microcalcifications Imaging Tip

Both microbleeds and microcalcifications appear hypointense on SWI-like sequences. Although it is possible, in principle, to discriminate microbleeds from microcalcifications on the

basis of the phase shift, as described, this may be more challenging than expected in clinical routine. In general, small lesions with simple spherical configurations are often associated with a clear phase shift and reliably differentiated as either microbleeds or microcalcifications by using the dipole behavior of the magnetic field. However, larger and more geometrically complex lesions can display complex signal on phase images (Fig 6), which change from one section to the next. Therefore, discrimination of microbleeds from microcalcifications is less evident and sometimes inconclusive. Moreover, section thickness and sequence parameters influence the ability to use phase to make this determination. Ideally, QSM should be used to resolve this issue because it takes all phase information and maps into the source magnetic field that first produced the phase. In calcifications, the phase would be low contrast in a left-handed system (11). Veins or calcification in the pineal or choroid plexus gland can be used as references to help differentiate paramagnetic from diamag-

Table 1: Overview of Susceptibility-Sensitive Sequences for MRI Vendors

Handedness	Sequence Name	Paramagnetic: Probable Microbleed	Diamagnetic: Probable Microcalcification
Left-handed		Hyperintense on phase images	Hypointense on phase images
Siemens	SWI		
Canon	FSBB		
Philips	3D GRE raw data		
Right-handed		Hypointense on phase images	Hyperintense on phase images
United Neusoft	SWI		
GE Healthcare	SWAN		
Philips	3D SWIp		

Note.— FSBB = flow sensitive black blood, GRE = gradient echo, SWAN = susceptibility-weighted angiography, SWI = susceptibility-weighted imaging, SWIp = SWI with phase enhancement, 3D = three-dimensional.

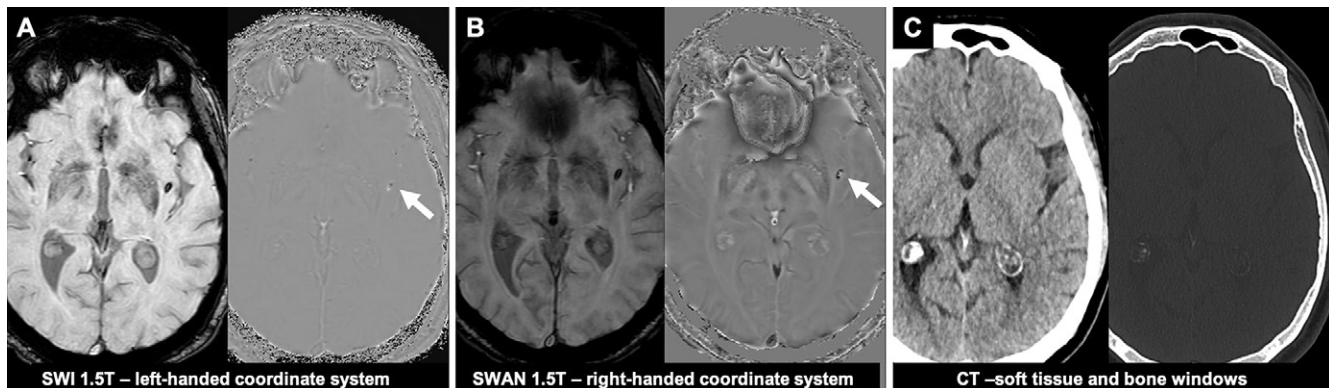


Figure 4: Difference between right-handed and left-handed coordinate systems in a patient with an ovaloid lesion at susceptibility-weighted imaging (SWI) in the left subinsular region. A, Phase image of a left-handed coordinate system shows a hypointense center and a hyperintense periphery (arrow). B, This susceptibility contrast is opposite on a right-handed coordinate system (arrow). C, CT confirms the absence of a calcification and consequently evokes a probable microbleed. SWAN = susceptibility-weighted angiography (GE Healthcare).

netic effects (Fig 7). Veins coursing in plane (perpendicular to the field) are diamagnetic in principle. But the effective phase gets reversed because of the thick sections and they may appear paramagnetic when the vein is small compared with the voxel size (12).

Handedness of MRI Systems Imaging Tip

Clinicians should always be aware of which handedness is used because that will affect the interpretation of phase shifts from blood (hemorrhage) versus calcium. QSM avoids the problem of handedness. One relatively simple and robust approach to determine the handedness is to assess the signal intensity of gray matter on the phase images. Gray matter is hyperintense on left-handed systems and hypointense on right-handed systems (Figs 5, E2 [online]).

Flow Compensation

All vendors can collect data by using a high-spatial-resolution three-dimensional gradient-echo sequence without flow compensation, especially by using multiechoes (where only the first TE can usually be fully flow compensated), whereas research sequences are available that apply full flow compensation to all echoes (Fig 7) (13). Conventional multiecho gradient-echo sequences have T2* weighting but no SWI processing.

Physiologic Factors Affecting Venous Signal

In a way, SWI-like sequences can be considered a high-spatial-resolution three-dimensional version of blood oxygen level-dependent imaging. Because these sequences use a long echo (which causes T2* dephasing from the venous signal specifically), any changes in oxygen saturation can cause a dramatic gain or loss of contrast in the images (usually much higher than that observed on blood oxygen level-dependent images). A good example is when you drink 2 cups of strong coffee or an energy drink with 200 mg of caffeine quickly. Within 20 minutes a peak effect of vasoconstriction (and therefore reduced perfusion) will occur with an increase in conspicuity of the veins (Fig 8). Similar local effects can occur in stroke with respect to viewing asymmetrically prominent cortical veins. Another clinical example is the diminished conspicuity during gestational age in children, possibly related to additional oxygen delivery by faster flow.

QSM and True SWI

The next evolution of susceptibility imaging is the development of QSM, allowing quantification of the magnetic susceptibility (3). QSM is an inverse process that operates on the filtered phase (Fig E3 [online]). The advantage of QSM is that the final quantitative result is theoretically not dependent on geometry, TE, or field strength (although the latter two affect

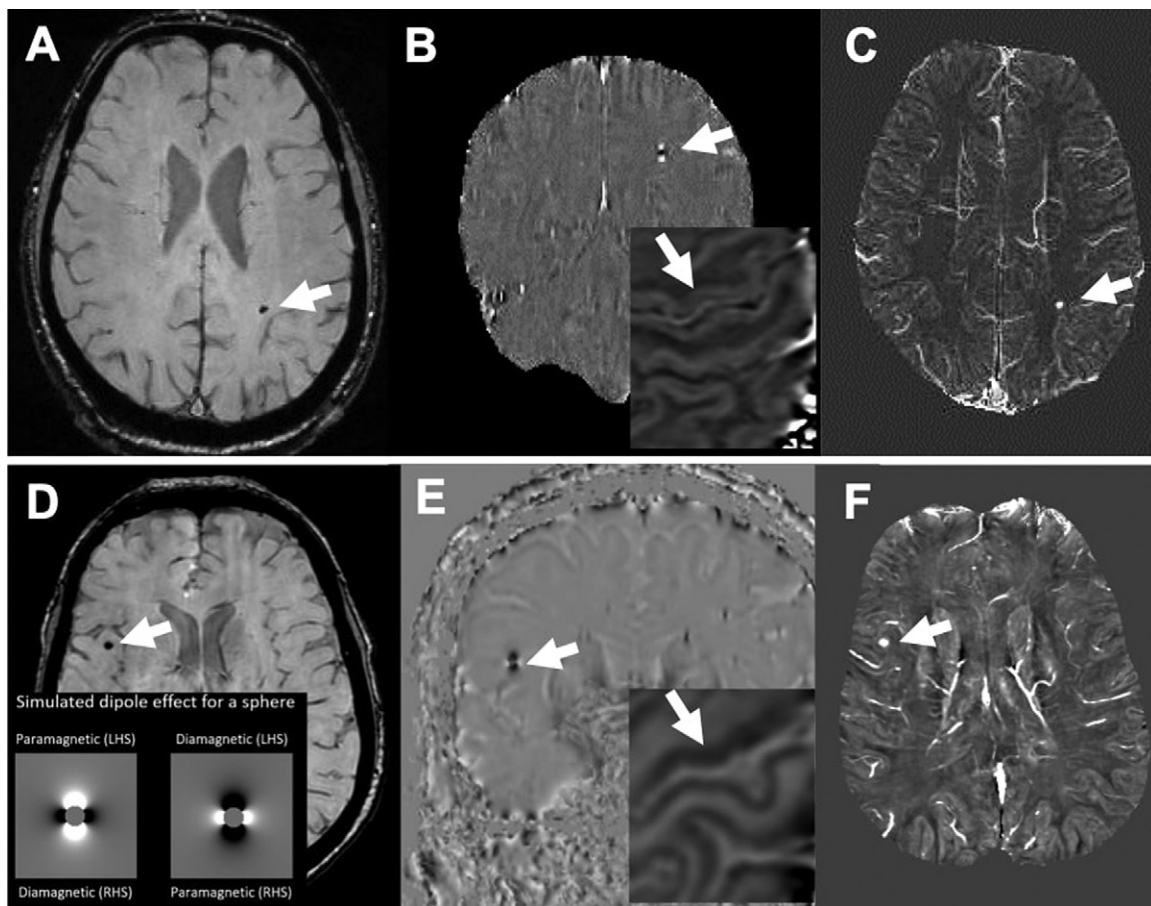


Figure 5: The use of the dipole effect and quantitative susceptibility mapping (QSM) to discriminate between microbleed versus microcalcification. *A*, On a left-handed system (LHS; 3.0-T susceptibility-weighted imaging), presence of one lesion (arrow) compatible with microbleed versus microcalcification. *B*, Corresponding dipole effect of the coronal phase image suggests microbleed (arrow). *C*, This is confirmed on the minimal intensity projection QSM as a hyperintense lesion (arrow). *D*, Companion case on a right-handed system (RHS; 3T susceptibility-weighted angiography [SWAN], GE Healthcare) shows the opposite dipole effect (arrow) on *E*, the coronal phase image (arrow), but *F*, the QSM is hyperintense (arrow), consistent with microbleed. The veins are hyperintense on QSM images regardless of whether they are derived from a right-hand or left-hand system. (Images courtesy of Dr Sagar Buch.) The signal intensity of the gray matter on phase images can be used to discriminate the handedness of a system: gray matter is hyperintense (arrow in *B* insert) in left-handed and hypointense (arrow in *E* insert) in right-handed systems.

the signal-to-noise ratio in the susceptibility maps). The phase mask in SWI is geometry dependent so it can lose susceptibility contrast. But if the QSM image is used to create the mask, the geometry dependence can be removed and we obtain what is referred to as a true SWI reconstruction (14), wherein veins are highlighted independent of their orientation (Fig 9).

Gadolinium Chelate–enhanced SWI

Gadolinium chelate–enhanced SWI does not require administration of intravenous gadolinium chelate. As an analogy, fluid-attenuated inversion recovery sequences are usually performed without administrating gadolinium chelate, yet clinical experience has demonstrated that fluid-attenuated inversion recovery with gadolinium chelate is useful for the depiction of meningeal disease. Likewise, first applications emerged by using SWI after injection of gadolinium-based contrast agent, suggesting SWI with gadolinium chelate is even more sensitive than normal SWI in depicting arteriovenous shunt (15). SWI with gadolinium chelate is not an established clinical tool, but this might change in the future.

Susceptibility-Tensor Imaging

Susceptibility-tensor imaging is the next technical development, allowing for the determination of orientation-dependent magnetic susceptibility parameters (16). In principle, it is similar to diffusion-tensor imaging and might eventually allow three-dimensional mapping of brain white matter fiber orientations. This technique is still awaiting clinical application.

Summary of Technical Issues and Clinical Hints for the Application of SWI

The choice of imaging parameters will affect signal-to-noise ratio, contrast, spatial resolution, and visibility of the structures of interest (17). The flip angle is particularly important because it determines the contrast, image quality, and signal-to-noise ratio on the images. A low flip angle (lower than the Ernst angles for gray matter and white matter) increases cerebrospinal fluid signal and reduces motion artifacts from inflow at the expense of signal-to-noise ratio (7). A summary of the recommended imaging parameters is shown in Table E1 (online). There are technical differences between MRI sequences

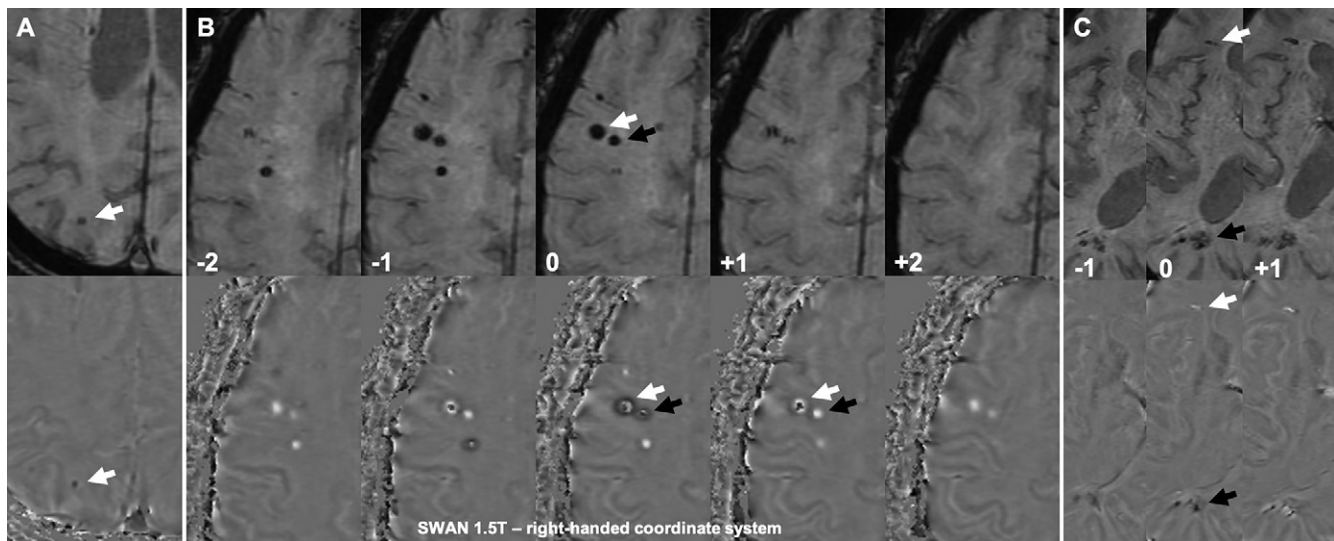


Figure 6: Clinical example of a patient with multiple probable microbleeds to demonstrate the effect of size and geometry of cerebral microbleeds on the phase images. A, A single punctiform lesion (arrows) has a clear hypointense signal on the phase image and is readily recognized as a microbleed in a right-handed MRI system. In lesions that are geometrically more complex, the interpretation of the phase images to discriminate microbleeds versus microcalcifications is less evident and may be inconclusive. B, Larger lesions have more complex appearance on phase images with partially hypointense (white arrows) and partially hyperintense signal (black arrows), which changes over sections (-2 to +2 on images). C, The same patient has more linear lesions (arrows) in frontal and parietal regions with radial orientation and more complex and discordant changes on the phase masks. SWAN = susceptibility-weighted angiography (GE Healthcare).

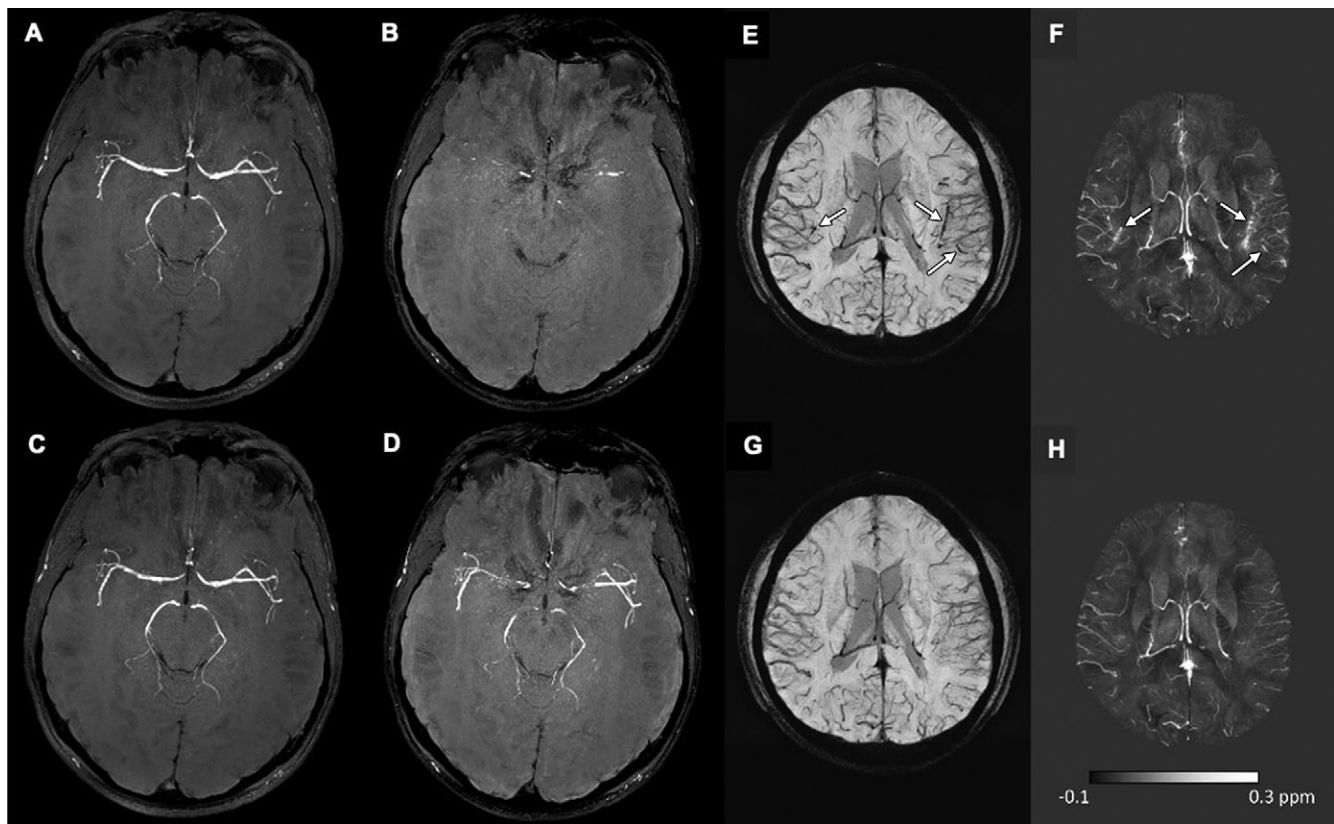


Figure 7: Multiecho susceptibility-weighted imaging (SWI) with and without flow compensation on the second echo. The short echo for most manufacturers is flow compensated (and for Siemens fully flow compensated for SWI) but the later echoes are not at, or are at most in, the read direction. In this example, the first echo is 7.5 msec (A, C) and the second echo is 17.5 msec (B, D). The lower row is fully flow compensated for all echoes, whereas the top row is from the manufacturer's clinical sequence with the same two echoes. The problem with not flow compensating the second echo (which is most useful for SWI) is that there can be remnant phase information in the arteries, and this can lead to artifacts in both the SWI and QSM data (arrows on E, F), which do not appear with the fully flow compensated data (G, H). (Images courtesy of Dr Yongsheng Chen, Wayne State University, Detroit, Mich.)

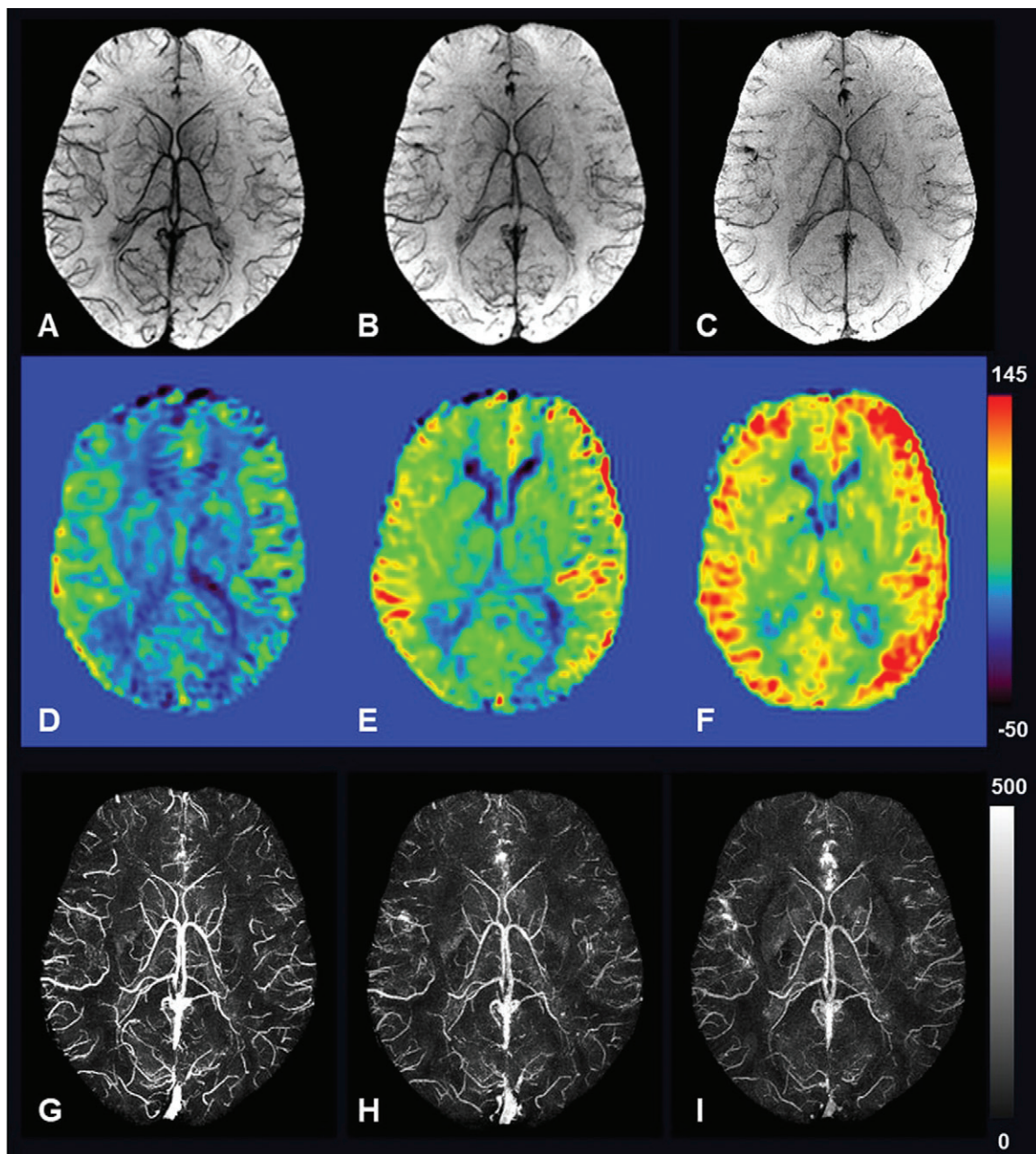


Figure 8: A–C, Minimum intensity projection of susceptibility-weighted imaging (SWI) data, D–F, cerebral blood flow maps, and, G–I, maximum intensity projection of quantitative susceptibility mapping (QSM) data show the dynamic changes in venous oxygen saturation because of, A, D, G, the administration of 200 mg of caffeine and, C, F, I, 1000 mg of acetazolamide. Minimum and maximum intensity projection images were projected over 64 sections or section slab with effective section thickness of 32 mm. The scale bar values for cerebral blood flow and QSM data are in milliliters per 100 g of tissue per minute and parts per billion. SWI data were acquired by using the following parameters: echo time msec/repetition time msec, 15 /24; flip angle, 15°; bandwidth, 119 Hz per pixel; and voxel resolution, $0.5 \times 0.5 \times 0.5 \text{ mm}^3$. (Images courtesy of Dr Sagar Buch.)

and vendors. The choice of imaging parameters is also dependent on field strength. The lower field strengths require longer TEs to acquire the same susceptibility effect (if the product of $\text{TE} \cdot B_0$ is constant, the susceptibility effects will be the same across field strengths) and, therefore, longer repetition time and lower signal-to-noise ratio. But higher field strengths can use a shorter TE and repetition time and have better signal-to-noise ratio. This makes SWI particularly effective and safe at high field strengths because it uses a low flip angle, and the specific absorption rate is lower than conventional spin-echo

sequences. Generally, a flow-compensated sequence will have fewer ghosting artifacts, especially when low flip angles are used. Multiple-echo SWI can also be used to allow for higher quality susceptibility mapping and $T2^*$ calculations. Finally, high in-plane resolution will produce the best results for viewing the small medullary veins.

Clinical Applications

SWI-like sequences were initially mostly used to improve the depiction of lesions and signs already known from standard

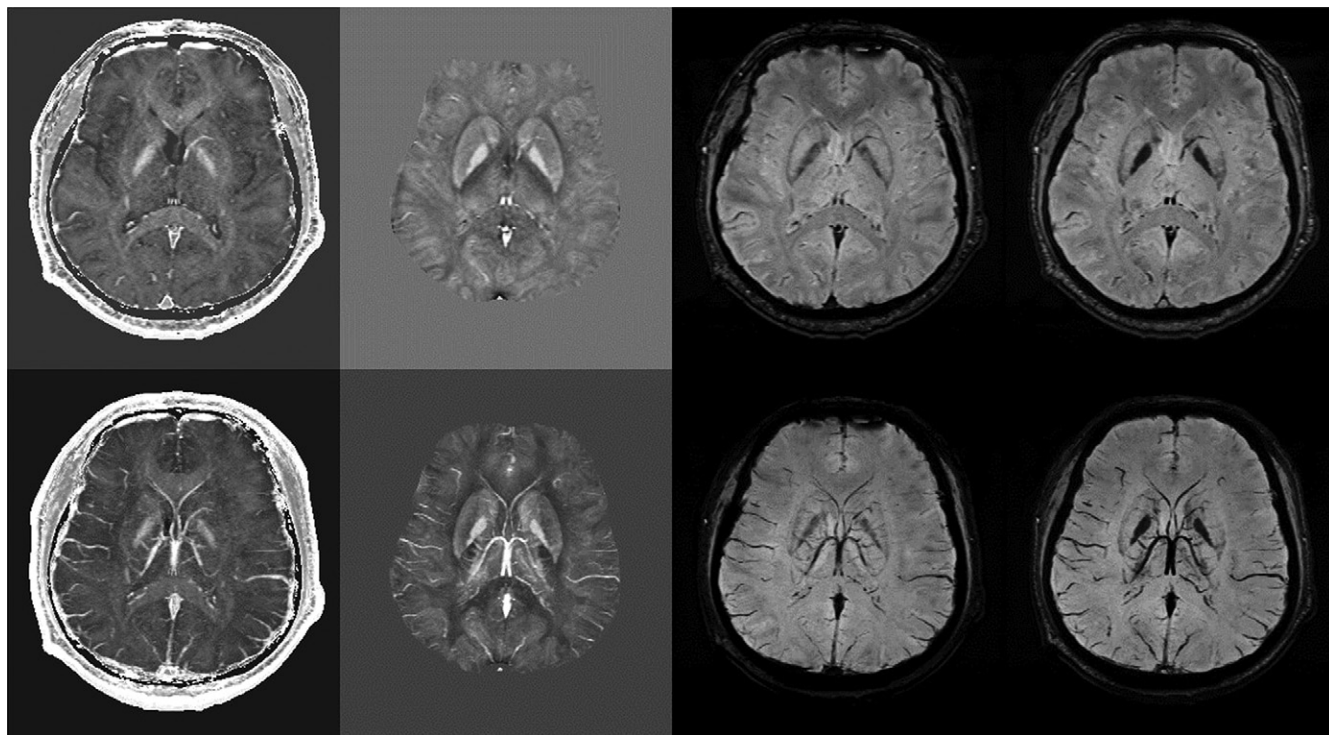


Figure 9: Example data set shows R2*, q, susceptibility-weighted imaging (SWI), and trueSWI. Top row: single section for (left to right) R2*, quantitative susceptibility mapping (QSM), SWI, and trueSWI (trueSWI is postprocessing for the same data set that avoids geometry-induced phase variation by using the source magnetic susceptibility as a mask). Bottom row: maximum intensity projection over eight sections for (left to right) R2*, QSM, minimum-intensity projection for SWI, and trueSWI (with improved overall contrast).

T2*-weighted imaging such as a higher number of microbleeds detected in aging, dementia, or mild brain trauma. Meanwhile, several additional clinical signs emerged specific to SWI-like sequences because of the increased susceptibility contrast and spatial resolution. These findings are not visible on standard T2*-weighted images with generally lower spatial resolution and two-dimensional acquisitions. Our review focuses on signs specific for SWI-like sequences.

Nigrosome 1 Sign in Parkinson Disease, Atypical Parkinsonian Syndromes, and Dementia with Lewy bodies

Parkinson disease.—Parkinson disease (PD) is the most common degenerative movement disorder. Standard MRI pulse sequences do not contribute to the diagnosis of PD. Diagnosis at imaging is on the basis of striatal dopamine uptake deficiency depicted by using nuclear medicine techniques, including ^{123}I -Ioflupane SPECT, also known as DaTScan. With the advent of SWI-like sequences, imaging of the nigrosome 1 (N1) became feasible first at 7.0 T but later also at 3.0 T. The N1 territory is located at the posterior part of the substantia nigra and characterized by a high signal intensity on high-spatial-resolution SWI-like sequences, flanked by two hypointense linear regions, which resembles a swallow tail (18) (Fig E4 [online]). Because of the neurodegeneration in PD, the hyperintense high-contrast spot of the N1 disappears, and only a single black region remains. It is unclear whether the disappearance of the high-contrast spot of the N1 is because of accumulation of iron leading to hypointensity, a volume loss of the N1 and resulting

approximation of the two flanking low-contrast borders, or a combination of both.

Clinical symptoms are often asymmetric in early stages of PD, and the dopamine uptake at dopamine imaging can be correspondingly asymmetric in the contralateral hemisphere. The N1 behaves similarly and may also show asymmetric abnormality in the contralateral hemisphere (19).

PD versus atypical parkinsonian syndromes.—On clinical grounds, the discrimination of PD versus atypical parkinsonian syndromes (APS) (eg, multisystem atrophy, multisystem atrophy putaminal type, multisystem atrophy cerebellar type, progressive supranuclear palsy, and corticobasal degeneration) may be challenging at early stages of the disease. Such a discrimination is relevant regarding prognosis and treatment. Dopamine imaging of the striatum and imaging of the N1 are abnormal in both PD and APS and cannot help to discriminate them (20). Structural MRI may depict additional imaging signs in APS (Table 2).

Consequently, the combination of N1 abnormalities at imaging and structural imaging results in a suggested decision tree differential diagnosis for PD and APS (Fig 10).

PD versus essential tremor and drug-induced parkinsonism.—At early stages of the disease in particular, the differential diagnosis of PD includes essential tremor and drug-induced parkinsonism. Dopamine imaging and the N1 are normal in both essential tremor and drug-induced parkinsonism (21,22). Unlike APS, there tend to be no other clinically significant structural brain abnormalities at MRI.

Table 2: Summary of Key Imaging Findings

Disease	N1/Dopamine Imaging	Other Imaging Findings
PD		
Findings	Abnormal (18)	None* (18)
Accuracy (%)		96
Sensitivity (%)		100
Specificity (%)		95
Dementia with Lewy bodies		
Findings	Abnormal (23–25)	None (24,25)
Accuracy (%)		76/90
Sensitivity (%)		63/93
Specificity (%)		79/87
APS (all)		
Findings	Abnormal (20)	Dopamine imaging and N1 are abnormal in PD and APS and cannot readily discriminate between PD versus APS
APS-PSP		
Findings		Midbrain atrophy (penguin sign, hummingbird sign, drooping Lilly sign)
APS-MSA-P		
Findings		Putaminal atrophy, putaminal iron deposition, peri-putaminal slit sign/peri-putaminal rim sign
APS-MSA-C		
Findings		Cerebellar and pontine atrophy, hot cross bun sign
APS-CBD		
Findings		Variable: parietal and cerebellar atrophy
Essential tremor		
Findings	Normal (21)	None (21)
Sensitivity (%)		94
Specificity (%)		75–88
Drug-induced parkinsonism		
Findings	Normal (22)	Normal (22)
Accuracy (%)		94
Sensitivity (%)		100
Specificity (%)		85

Note.—Summary is of key imaging findings in Parkinson disease, dementia with Lewy bodies, atypical parkinsonian syndromes including progressive supranuclear palsy, multisystem atrophy putaminal type, multisystem atrophy cerebellar type, corticobasal degeneration, and differential diagnoses of essential tremor and drug-induced parkinsonism. APS = atypical parkinsonian syndrome, CBD = corticobasal degeneration, MSA-C = multisystem atrophy cerebellar type, MSA-P = multisystem atrophy putaminal type, N1 = nigrosome 1, PD = Parkinson disease, PSP = progressive supranuclear palsy.

*Abnormality is often asymmetric at early stages of the disease (19).

Dementia with Lewy bodies.—Lewy body accumulation occurs in both dementia with Lewy bodies and PD, which are considered to be a spectrum of disorders. If cognitive symptoms predominate, the clinical diagnosis is dementia with Lewy bodies. If motor symptoms predominate, the clinical diagnosis is PD, with clinical symptoms partially overlapping and evolving over time. Having shared underlying pathologic structure, dopamine imaging findings show abnormalities in PD and dementia with Lewy bodies. Likewise, the N1 is also abnormal in dementia with Lewy bodies (23–25). In the absence of other reliable structural markers at MRI for dementia with Lewy bodies, imaging of the N1 may resolve this so-called blind spot of MRI (Fig 11).

Technical considerations in imaging the N1.—It is challenging to image and evaluate the N1 sign and requires both a high-quality high-spatial-resolution SWI-like sequence and an experienced reader (26). The degeneration of N1 is not a binary

normal or abnormal phenomenon but a continuous process. We therefore proposed a gradual rating scale from definitely normal to probably normal to probably abnormal to definitely abnormal (24) (Fig E5 [online]). In addition to the gradual abnormality described, there is also normal interindividual anatomic variability (26) (Fig 12).

In general, imaging at 3.0 T is preferred because of the ability to obtain higher spatial resolution with good signal-to-noise ratio, but imaging at 1.5 T may be achievable (24). Reduction of section thickness from 2 mm to 1.5 mm (3.0 T) or 1.6 mm (1.5 T) improved accuracy from 67% to 84% (24). Moreover, the appearance of the nigrosome is somewhat variable between vendors and even within a vendor from scanner to scanner (Fig 13).

In some patients, the N1 appears abnormal without clinical symptoms. It remains to be determined whether this represents a false-positive finding or signifies preclinical disease (as known from dopamine SPECT). Nevertheless, recent studies (26) have

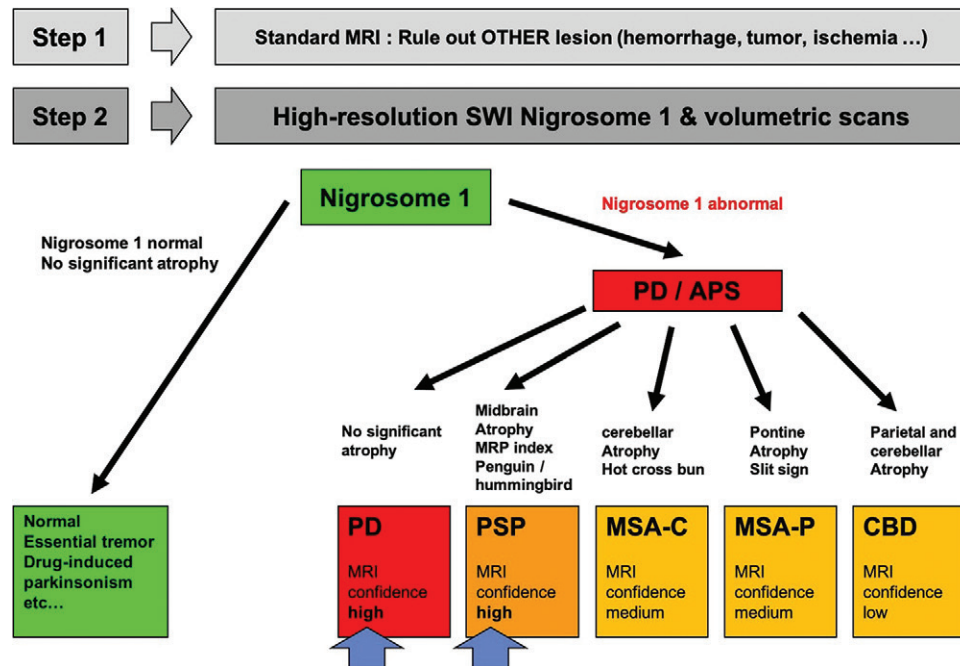


Figure 10: Schematic evaluation of nigrosome 1 (N1) in Parkinson disease (PD) and atypical parkinsonian syndrome (APS). Step 1 is to first rule out other pathologic causes by using standard imaging and then, step 2, evaluate N1. If N1 is abnormal, then check for focal atrophy to discriminate between PD and atypical parkinsonian syndrome. CBD = corticobasal degeneration, MSA-C = multisystem atrophy cerebellar type, MSA-P = multisystem atrophy putaminal type, PSP = progressive supranuclear palsy, SWI = susceptibility-weighted imaging.

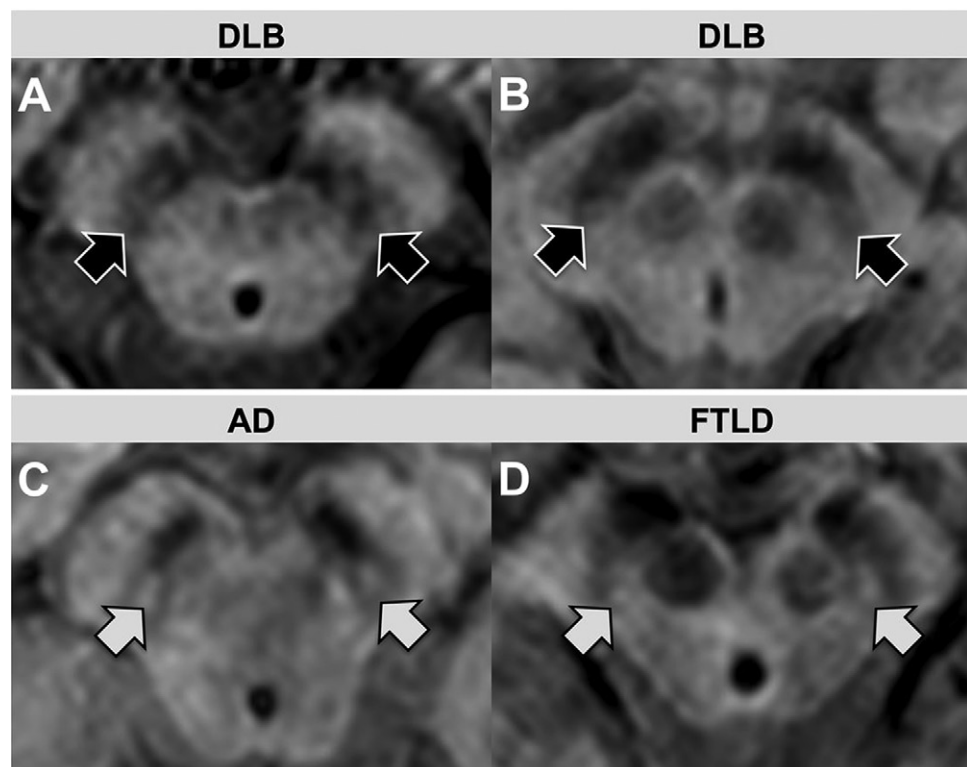


Figure 11: A–D, illustration of, A, abnormal nigrosome 1 (N1; black arrows) in patients with dementia with Lewy bodies (DLB), yet normal N1 (white arrows) in other types of dementia including Alzheimer dementia (AD) and frontal dementia/frontotemporal lobar degeneration (FTLD). (Reprinted and adapted, with permission, from reference 23.)

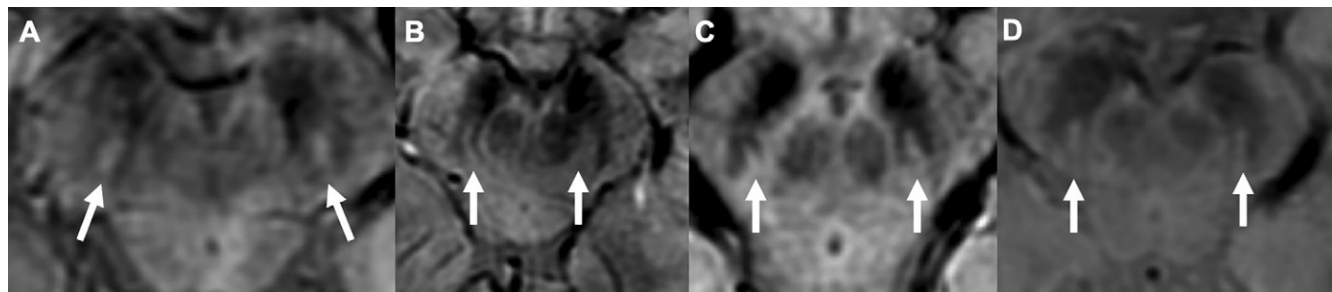


Figure 12: Anatomic variation (arrows) in the appearance of the nigrosome 1 (N1). On the 3.0-T axial plane, susceptibility-weighted angiography (SWAN; GE Healthcare) shows, A, ovoid appearance; B, bow-like [ie, banana-shaped] appearance; C, triangular appearance; and D, in younger patients, the substantia nigra is less hypointense because of lower iron content and the high contrast of the N1 is less evident.

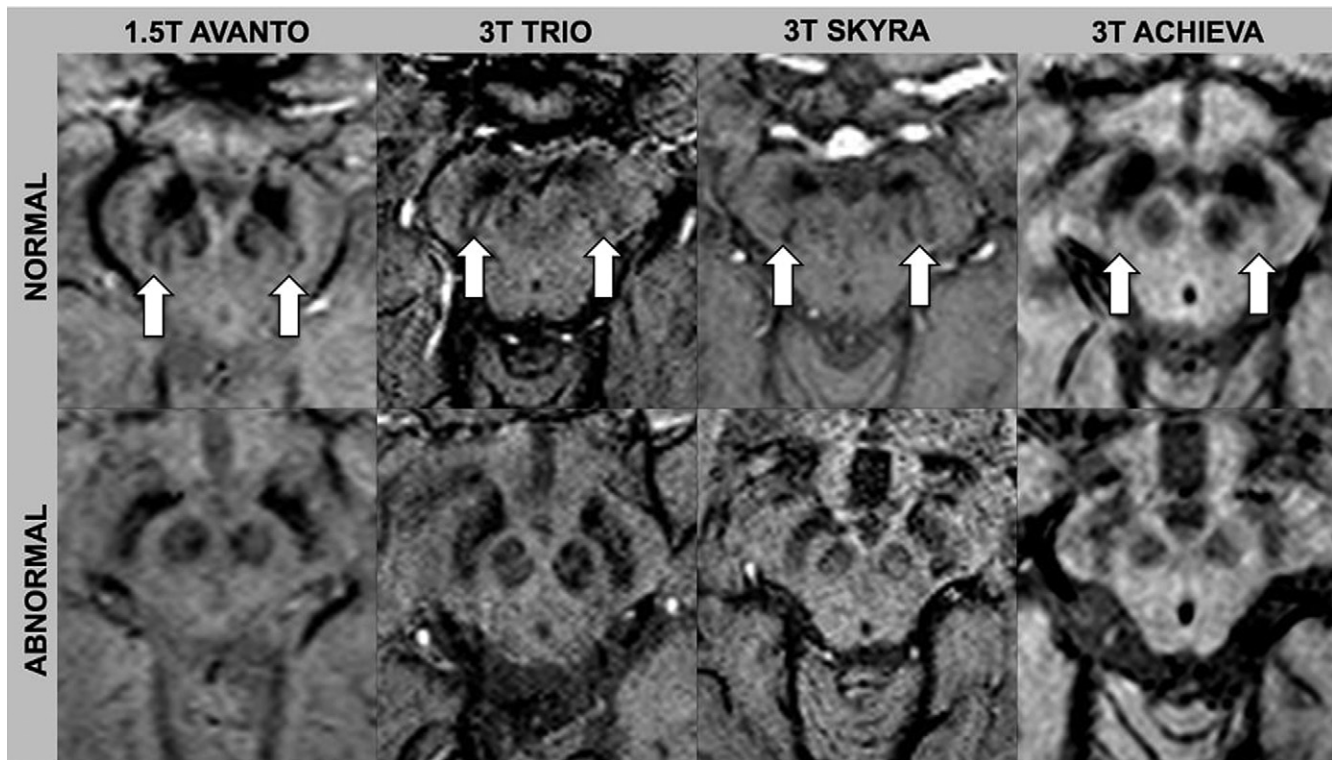


Figure 13: Different vendors, sequences, and imaging parameters can lead to slightly different appearance of the nigrosome 1 (arrows). (Reprinted and adapted, with permission, from reference 24.)

shown that although there is a high sensitivity in distinguishing patients with PD from healthy control patients if the N1 sign has disappeared, there remain false-negative findings where the N1 sign has not disappeared. Overall, however, the rate of true-negative findings is high.

The central vessel sign and peripheral rim sign in multiple sclerosis.—Multiple sclerosis is a demyelinating disorder caused by perivenular inflammation. Imaging criteria rely on the location of T2-weighted hyperintense lesions and contrast-enhanced lesions, which have important roles in diagnostic criteria (27). In some cases of patients suspected of having multiple sclerosis, notably in somewhat older patients with cardiovascular risk factors, it may be difficult to discriminate vascular-ischemic from demyelinating lesions. The central vessel sign is characteristically found in multiple sclerosis lesions by findings that show venous structures as a linear

hypointensity on SWI scans in the center of the lesion (often aligning with the main longitudinal axis of ovoid lesions). The central vessel sign is best depicted on 3.0-T scans but not fully specific for multiple sclerosis, occurring in 40.9% of multiple sclerosis lesions and in 27.2% of vascular lesions (28). A cut-off greater than 45% in brain lesions with central vessel sign was suggested to discriminate multiple sclerosis from vascular (or other) lesions (28) (Fig 14).

Other features at SWI-like imaging in multiple sclerosis include central signal loss and the so-called hypointense rim sign (Fig 15). The latter has been linked to deposition of iron in macrophages and may reflect chronically active multiple sclerosis lesions. Rim lesions are best detected at 3.0 T or higher and are associated with more destructive features at MRI and a worse clinical prognosis (29).

Another related imaging sequence, fluid-attenuated inversion recovery, which combines a T2-weighted fluid-attenuated

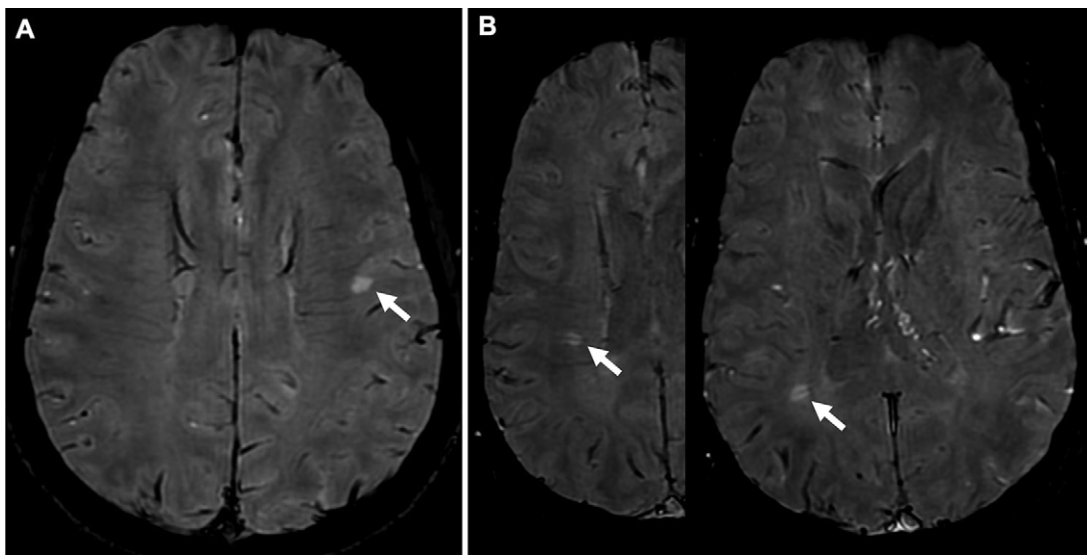


Figure 14: Images from 3.0-T axial plane susceptibility-weighted angiography (SWAN; GE). *A*, Image in a 41-year-old man with multiple vascular risk factors. The white matter lesion (arrow) did not have a central vessel sign. *B*, Images in a 41-year-old man with first diagnosis of multiple sclerosis. The majority of white matter lesions had a central vessel sign (arrows).

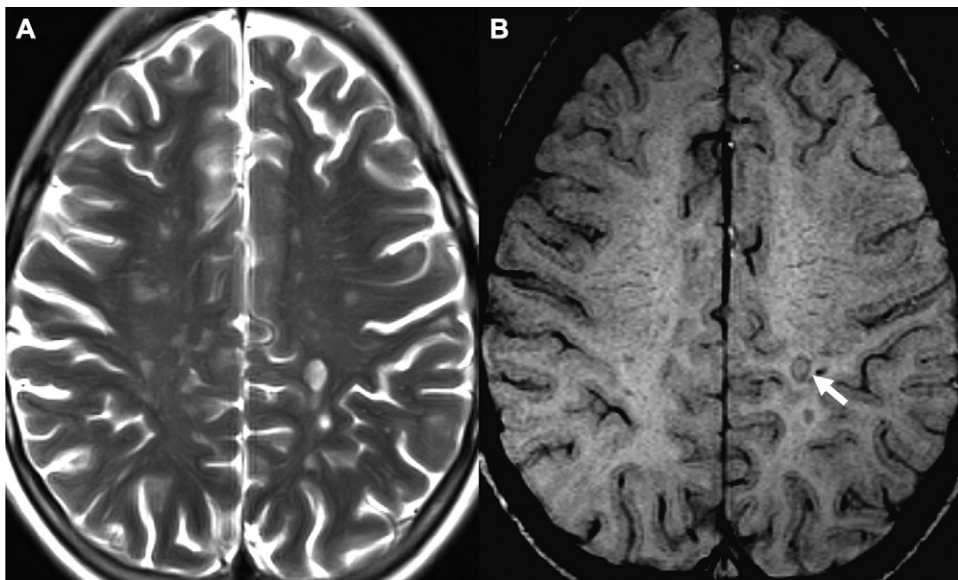


Figure 15: *A*, Image in a 16-year-old girl with known multiple sclerosis. *B*, In a minority of lesions, a peripheral rim sign (arrow) is present. It is an emerging sign currently thought to reflect iron deposition in macrophages in chronically active multiple sclerosis lesions.

inversion recovery contrast and T2*-weighted contrast in a single image (30), allows for simultaneous assessment of white matter lesions and the central vessel sign notably for evaluating multiple sclerosis lesions.

Progressive multifocal leukoencephalopathy.—Progressive multifocal leukoencephalopathy is a subacute progressive infection in the central nervous system that is from reactivation and replication of JC virus. The disease is associated with the human immunodeficiency virus and acquired immunodeficiency syndrome, and other immunocompromised or immunosuppressed patients, now commonly observed in patients

with multiple sclerosis who are treated with immunomodulatory drugs. A thin, uniformly linear, gyriform rim that is hypointense at SWI in the paraleisional U-fibers occurs in patients with multiple sclerosis and definite progressive multifocal leukoencephalopathy, representing an end-point stage of the neuroinflammatory process in long-term survivors (31). Infratentorial progressive multifocal leukoencephalopathy lesions showed no signs of hypointense rim formation at SWI. One possible explanation for the specific location of SWI findings is the greater iron content in subcortical fibers and high density of iron-rich oligodendrocytes. The prognostic relevance of a hypointense rim

at SWI in progressive multifocal leukoencephalopathy needs to be established (Fig 16).

Susceptibility vessel sign in acute arterial stroke.—In acute stroke with arterial vessel occlusion, SWI-like sequences may depict clot-related susceptibility changes known as the susceptibility vessel sign (Fig E6 [online]). For the prognosis of intravenous thrombolysis in acute stroke, a thrombus length longer than 8 mm identified by using SWI-like sequences predicts an unfavorable outcome (32). However, with the increasing application of endovascular treatment of acute stroke, the length of the thrombus is less relevant and not correlated with outcome

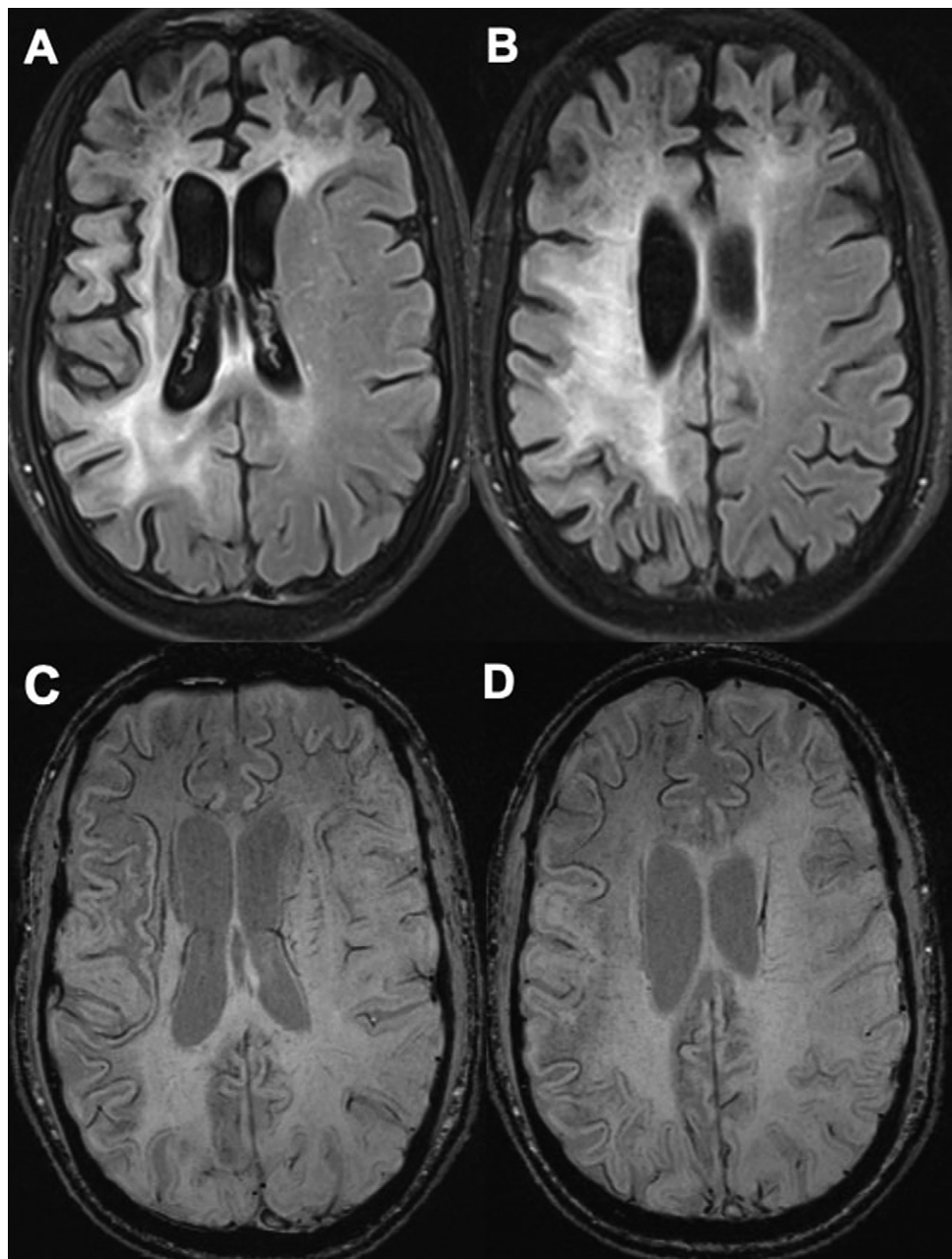


Figure 16: MRI scans in a 31-year-old man who is positive for HIV and has confirmed progressive multifocal leukoencephalopathy. A, B, On axial fluid-attenuated inversion recovery MRI scans, high signal intensity abnormality is observed in the frontal lobe on both sides and in the white matter of the right hemisphere. C, D, On corresponding susceptibility-weighted images, a linear hypointensity is on the cortical side of the progressive multifocal leukoencephalopathy lesions.

(33). Moreover, the susceptibility vessel sign may be variable in appearance (eg, because of technical differences between SWI-like sequence implementation).

Asymmetrically prominent cortical veins.—Deoxyhemoglobin acts as an endogenous susceptibility agent to increase venous conspicuity. In the acute stage of ischemic stroke, arterial occlusion greatly reduces oxygen delivery. As brain tissue continues to use the oxygen in the area of reduced perfusion, the relative concentration of deoxyhemoglobin increases, causing cortical veins in the affected area to appear larger and lower contrast on SWI-like sequences, which creates asymmetrically prominent cortical veins (34) accompanied by

a potential physiologic response that physically increases the diameter of the veins in the region. The asymmetrically prominent cortical vein territory matches the affected territory seen on mean transit time images. If perfusion is restored and mean transit time returns to normal, usually the asymmetrically prominent cortical veins sign vanishes, indicating that the blood oxygen saturation in that region has returned to normal. Comparing the region occupied by asymmetrically prominent cortical veins with that seen on diffusion- or perfusion-weighted images can help predict infarct size growth and outcome. Diffusion and perfusion mismatch predicts a favorable response to treatment. But the use of asymmetrically prominent cortical vein region as a third measure adds a physiologic component not considered in the other two modalities: oxygen extraction fraction. SWI and diffusion-weighted imaging mismatch has been strongly related to perfusion- and diffusion-weighted imaging mismatch (35,36), suggesting a role for SWI-like sequences in conjunction with standard stroke sequences (Fig 17).

The presence or absence of asymmetrically prominent cortical veins may correlate with infarct size and outcomes. The presence of any subtype of asymmetrically prominent cortical veins can be associated with poor outcome regardless of therapy (37). Most studies have been retrospective and

bound by the 6-hour period of treatment. For patients outside of that period, no viable treatment changes on the basis of SWI exist beyond antiplatelet therapy. Studies that correlate the asymmetrically prominent cortical vein finding with a worse outcome may involve patients who have persistent-misery perfusion without the ability to treat it because of the 6-hour time limit. A poor outcome is predictable in that scenario because a penumbra with a high oxygen extraction fraction (showing asymmetrically prominent cortical veins) goes untreated because of the short treatment time and, therefore, the infarct grows in size. SWI for acute stroke is not commonplace because of logistical priorities at most stroke centers that focus on

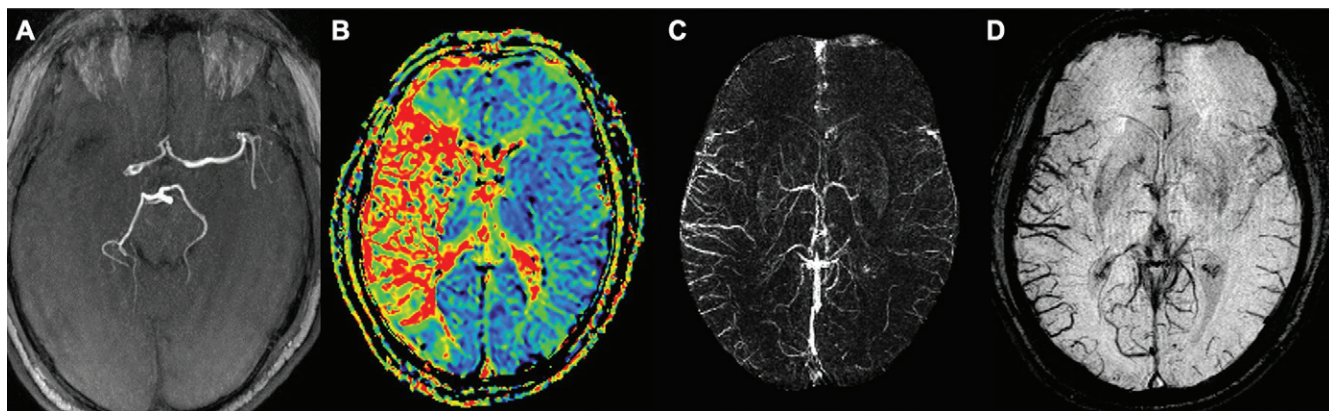


Figure 17: Patient with stroke and asymmetrically prominent cortical veins. **A**, Time-of-flight angiographic image shows a severely occluded right middle cerebral artery. **B**, Perfusion MRI scan shows that the mean transit time was affected in most of the right hemisphere. **C**, Many asymmetrically prominent cortical veins are evident on the quantitative susceptibility map maximum intensity projection image and **D**, susceptibility-weighted image. The asymmetrically prominent cortical veins represent the area with a reduction in perfusion and subsequent increase in deoxyhemoglobin, delineating where a salvageable penumbra exists. Acquisition parameters at 1.5-T SWI were as follows: repetition time msec/echo time msec, 49/40; flip angle, 15°. (Images courtesy of Luo Yu, MD, and Miller Fawaz, MS.)

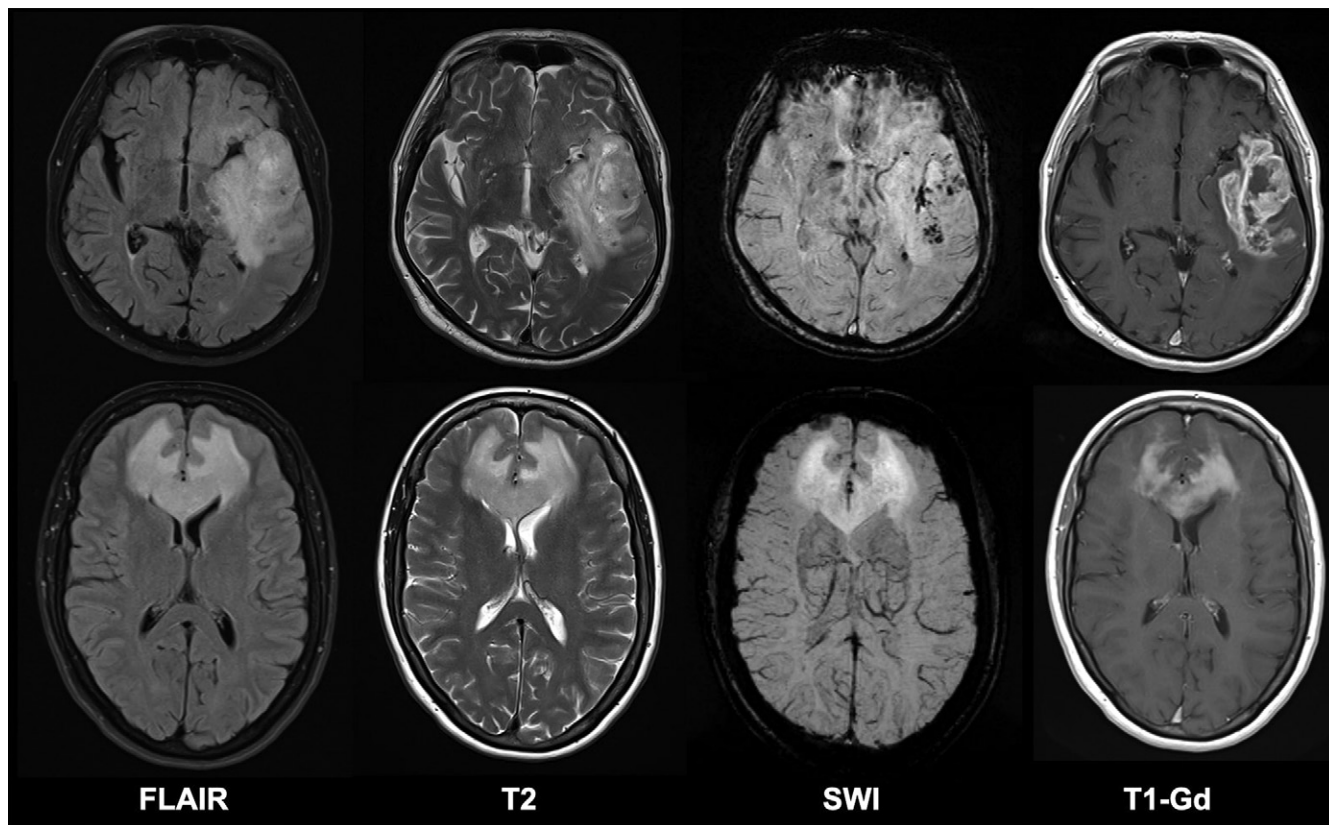


Figure 18: Images in a 74-year-old man who presented with aphasia and was found to have a high-grade left temporal glioma at 1.5-T MRI (top). Note the intratumoral susceptibility signals on axial susceptibility-weighted imaging (SWI), which indicated microhemorrhage and vessel proliferation. Images in a 57-year-old woman who presented with behavioral changes because of a lymphoma (bottom). SWI did not show any intratumoral susceptibility signals despite marked homogeneous enhancement. FLAIR = fluid-attenuated inversion recovery; Gd = gadolinium-chelate enhanced.

CT, but this area is expected to develop further now that MRI is increasingly performed at the acute phase in stroke centers.

Intratumoral susceptibility signals in neoplasms.—In brain tumors, SWI findings can reveal features that remain undepicted at conventional MRI, referred to as intratumoral susceptibility signals. These are linear or dot-like intratumoral areas of low sig-

nal on susceptibility images, most likely related to intratumoral microhemorrhage, calcification, and neovascularization. By using phase images, it is possible to identify calcifications (comparable to CT) linked specifically to oligodendrogloma. Intratumoral susceptibility signals occur in a high percentage of high-grade gliomas but are mostly absent in lymphoma (38). Within the group of gliomas, intratumoral susceptibility signals seem less able to help

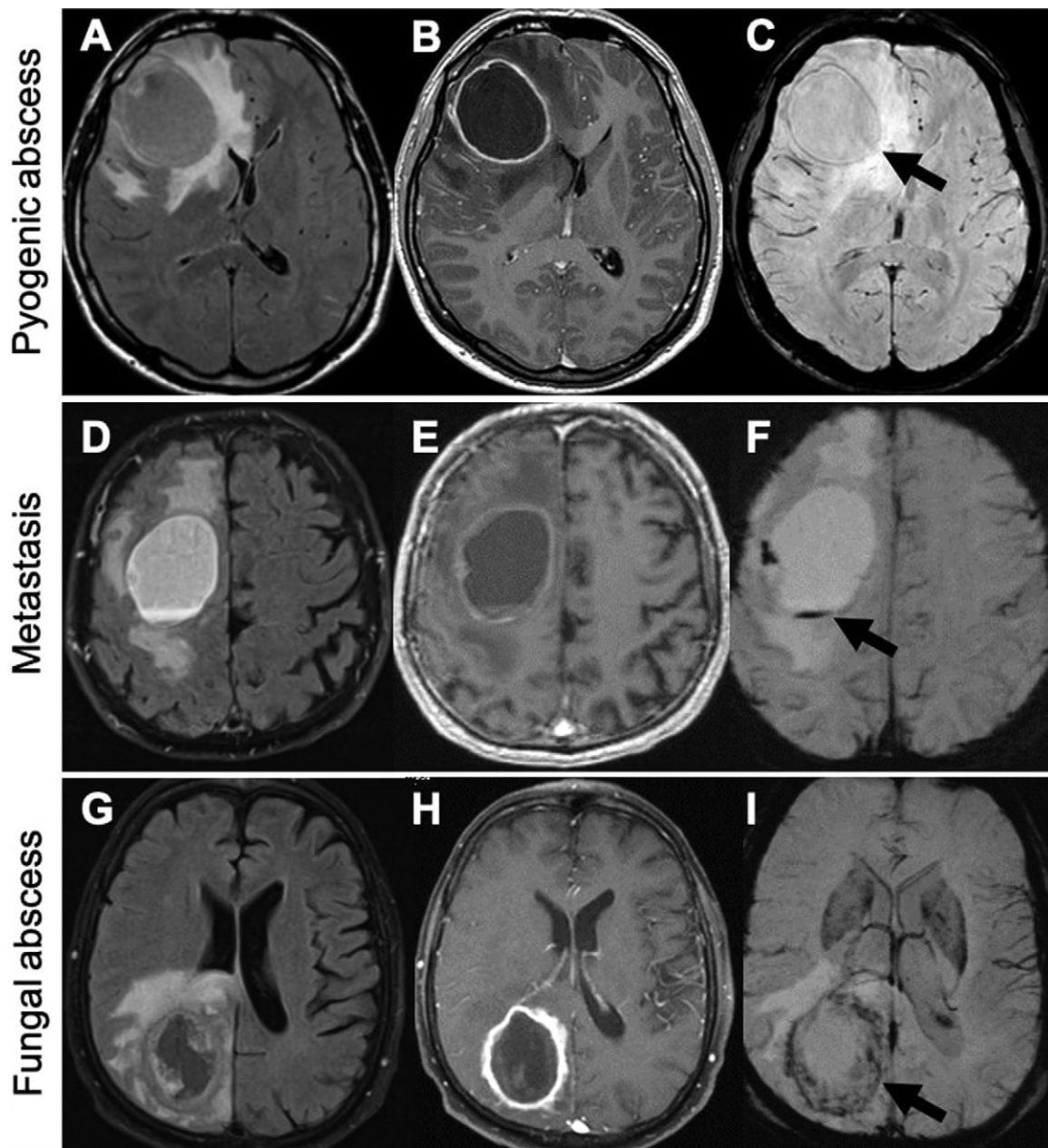


Figure 19: A–C, Axial susceptibility-weighted imaging (SWI) findings show a dual rim sign (arrow in C) in a pyogenic abscess consisting of a dark outer rim and a high-contrast inner rim. D–F, SWI findings do not show a dual rim sign but nodular hypointensity and blood level in brain metastasis manifesting as cystic ring-like enhancing lesion (arrow in F). G–I, SWI findings show peripheral marked hypointensity but no dual rim sign in a patient with a fungal abscess (arrow in I).

predict tumor grade than does perfusion MRI (39), but they are related to the isocitrate dehydrogenase 1 mutation status. A developed grading scale for intratumoral susceptibility signals (40) focuses on dot-like and fine linear intratumoral susceptibility signals only (grade 0, no intratumoral susceptibility signals; grade 1, one to five intratumoral susceptibility signals; grade 2, six to 10 intratumoral susceptibility signals; and grade 3, more than 10 intratumoral susceptibility signals), showing a good correlation with abnormal perfusion values (Fig 18).

Dual rim sign in abscess.—In cases of brain abscess, SWI can differentiate between pyogenic and fungal abscesses. This may also

be helpful diagnostic clue to discriminate the lesion versus other ring-enhancing lesions, notably glioblastoma or metastasis (41). More recently, a dual rim sign, the combination of a hypointense and a hyperintense rim, was proposed as a diagnostic sign in favor of pyogenic abscess, whereas a fungal abscess typically shows an ill-defined and thick hypointense rim (Fig 19) (42). Rarely dot-like and linear low-contrast areas at SWI, indicating hypervascularization, occur in pyogenic abscesses in the early capsular stage.

Imaging Signs with Enhanced Visibility on SWI-like Sequences
CMBs occur in a variety of diseases including aging and dementia (dementia from Alzheimer disease in particular) and

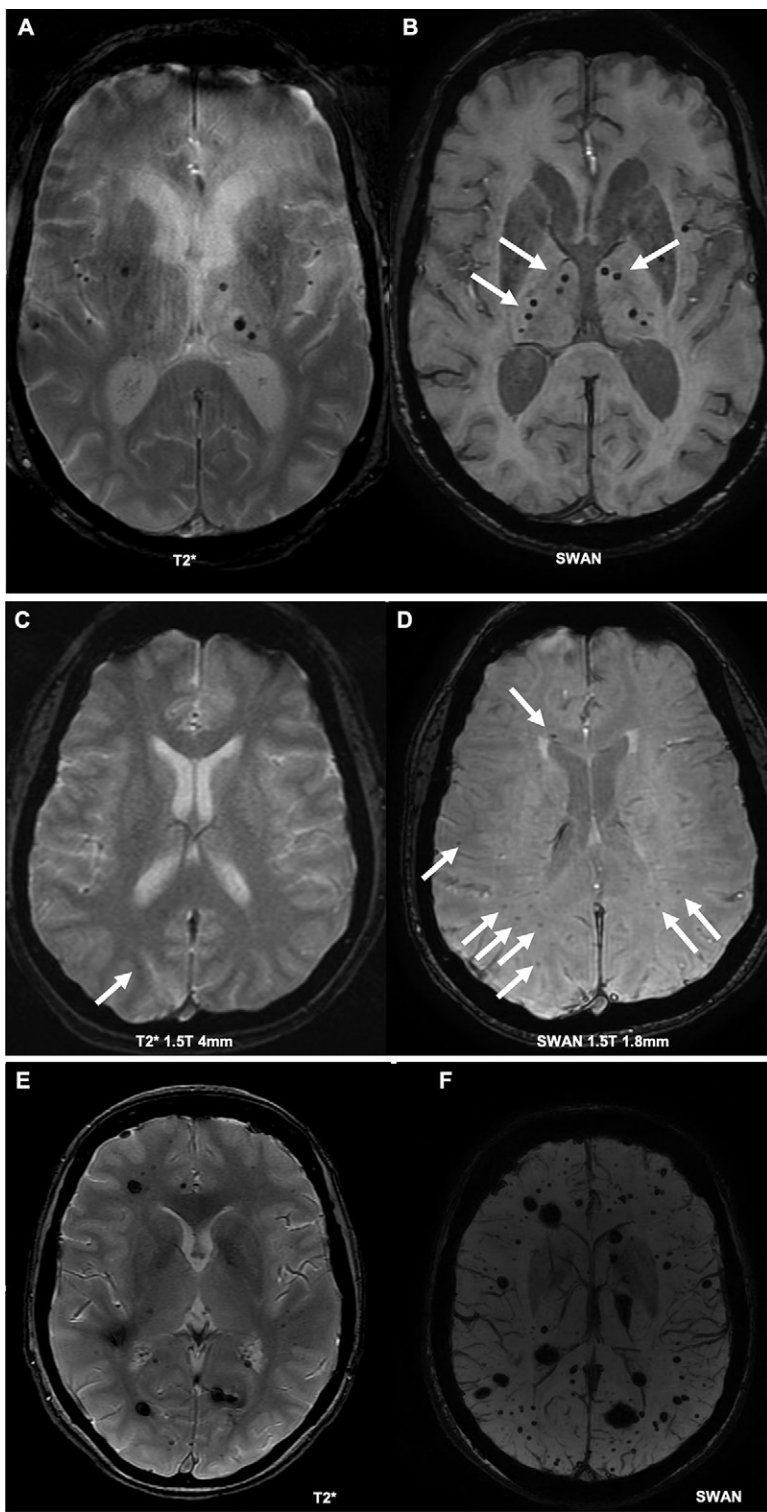


Figure 20: Imaging findings show the effect of technical parameters in the depiction of cerebral microbleeds (CMBs). A, B, CMBs (arrows in B) in typical location of thalamus in hypertension are more evident and more numerous at axial SWI compared with T2*-weighted imaging. C, D, Microbleeds/hemorrhagic diffuse axonal injuries in mild to moderate traumatic brain injury (arrows in C, D) are better depicted at susceptibility-enhanced imaging compared with T2*-weighted imaging (effect of susceptibility enhancement and section thickness). E, F, Small microcavernomas are radiologically indistinguishable from cerebral microbleeds, but the presence of associated larger size cavernomas in familial cavernomatosis allows for a correct diagnosis. SWAN = susceptibility-weighted angiography (GE Healthcare).

vascular disease. They are markers of vascular disease and may occur preferentially in specific spatial locations such as hypertensive CMBs typically in the basal ganglia or CMBs in cerebral amyloid angiopathy with a peripheral or lobar predilection. Imaging of CMBs is a key application of SWI-like sequences because in general more CMBs can be detected compared with routine T2*-weighted imaging. The detection rate of CMBs depends on field strength, section thickness, and type of susceptibility weighting. For example, in a memory clinic setting, 20% of individuals with mild cognitive impairment had CMBs on T2*-weighted images, but 40% had CMBs on SWI scans (43). CMBs occur in a variety of diseases, as discussed in detail in a recent review article (43) (Fig 20). Therefore, we only summarized the key imaging findings of CMBs in Table 3.

SWI in Traumatic Brain Injury

An important application of SWI-like imaging is the detection of hemorrhage in traumatic brain injury. In general, moderate and severe traumatic brain injuries have evident posttraumatic lesions visible on unenhanced CT images. The situation is fundamentally different in mild traumatic brain injury, where it can be challenging to depict posttraumatic lesions at neuroimaging (Fig 21). The depiction of microbleeds (hemorrhagic diffuse axonal injuries or shearing injuries in this context) is of key importance for patient prognostication but also from a medical and legal perspective. Similar to the discussion of microbleeds, SWI-like will depict more lesions than CT or standard T2* (44,45), and lesions remain visible for many years, even though their numbers may slightly reduce over time (46).

Diffuse axonal injury may be accompanied by diffuse vascular injury (47). Diffuse vascular injury visible at SWI consists of convergent-type hemorrhages in the supratentorial white matter distributed along the perimedullary veins, which drain into the septal vein (Fig 22). Existence of bead-like or convergent bead-like supratentorial hemorrhages (diffuse vascular injury) at SWI are associated with a poor outcome (47). The exact discrimination of diffuse axonal injury versus diffuse vascular injury and the clinical implications remains to be elucidated in future studies.

Superficial Siderosis

Superficial siderosis is another imaging sign observed at susceptibility imaging. It consists of linear signal loss following the pia on the surface of the brain, and when it occurs on either side of a sulcus it creates a tram-track sign. It is important to discriminate be-

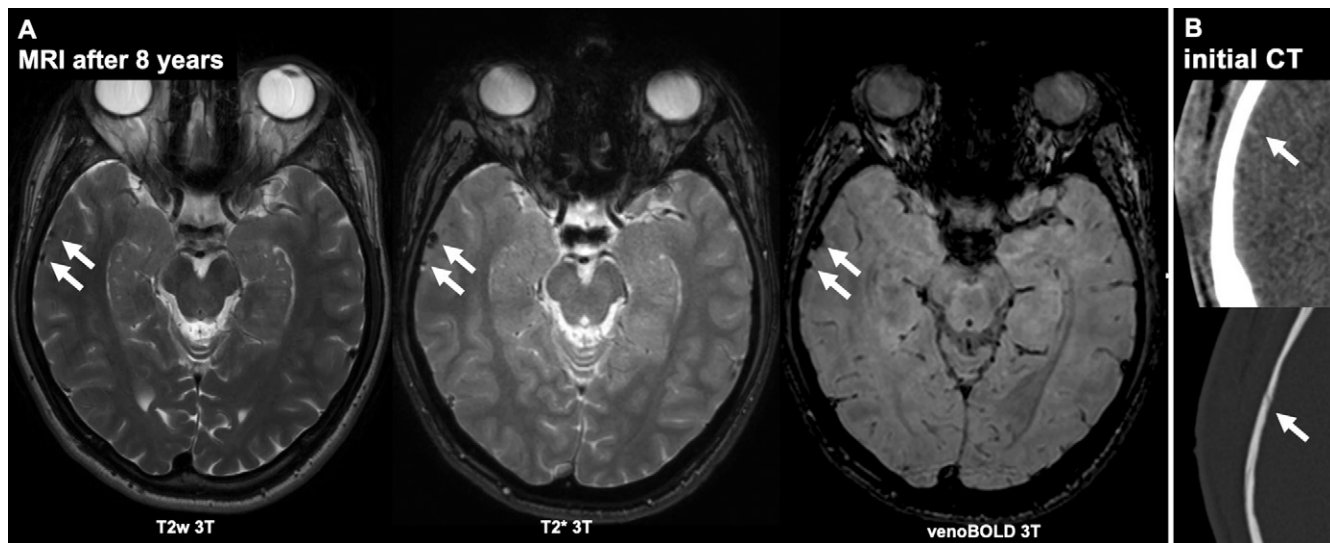


Figure 21: A, Findings from MRI performed 8 years after a minor trauma showed two hemosiderosis lesions (arrows), better appreciated at axial venous blood oxygen level-dependent imaging compared with axial T2*-weighted imaging. B, Findings from the initial CT on the day of the trauma show faint acute hyperdense bleeding of one lesion and a tiny skull fissure (arrows).

Table 3: Overview of Key Imaging Findings of Cerebral Microbleeds in Various Diseases

Disease	Key Imaging Finding
Aging/dementia	Lobar or central CMBs with/without other imaging findings of neurovascular or neurodegenerative diseases; ≥ 2 CMBs at T2* \geq three CMBs at susceptibility-weighted imaging probably abnormal and suggestive of Alzheimer or mixed dementia
Hypertensive microbleeds	Central distribution including basal ganglia and infratentorial region, often associated with other imaging findings of neurovascular diseases
CAA	Peripheral “lobar” distribution, typically sparing basal ganglia and infratentorial region, often associated with superficial siderosis, white matter anomalies, lacunes
CADASIL	Predilection of CMBs in basal ganglia, associated with other findings of CADASIL including white matter anomaly of temporal poles
Traumatic microbleeds	Also known as hemorrhagic diffuse axonal injuries or shearing injury, may have more ovoid configuration in radial distribution following the perivascular spaces
Microcavernoma	Microcavernomas may be indistinguishable from spontaneous cerebral microbleeds. In case of multiple cavernomas (familial cavernomatosis) larger lesions may show typical pop-corn appearance suggestive of cavernoma. Alternatively, some cavernomas may be associated with a developmental venous anomaly
Radiation-induced microbleeds	Typically occur in the field of radiation
ARIA-H	May occur in patients treated with amyloid-lowering therapies and in the acute stage may be associated with edema and white matter abnormalities

Note.—ARIA-H = amyloid-related imaging abnormalities—hemosiderin, CAA = cerebral amyloid angiopathy, CADASIL = cerebral autosomal dominant arteriopathy with subcortical infarcts and leukoencephalopathy, CMB = cerebral microbleed.

tween superficial (convexity), deep, and infratentorial locations (Fig E7 [online]). Superficial siderosis may occur in a variety of diseases. The most common causes are summarized in Table 4.

Neurodegeneration with Brain Iron Accumulation

Neurodegeneration with brain iron accumulation is a heterogeneous and evolving group of disorders related to brain iron accumulation notably in the basal ganglia. Most of these diseases are genetic. Neurodegeneration with brain iron accumulation is an evolving field. Therefore, terminology and disease classification are evolving as new diseases become added to this group. For an overview, see Kruer et al (48). Iron deposition can be depicted by using standard T2*-weighted imaging in

principle, but SWI-like sequences may provide more conspicuous findings. QSM has the potential of a more objective imaging marker in the future.

The so-called eye of the tiger (Fig 23) sign of the pallidum is the most well-known imaging marker and occurs typically in pantothenate kinase-associated neurodegeneration, formerly known as Hallervorden-Spatz disease. Other diseases have iron deposition with a slightly different distribution.

Motor Neuron Disease

Amyotrophic lateral sclerosis is the most common motor neuron disease affecting both upper and lower motor neurons. Typical imaging findings include high signal on

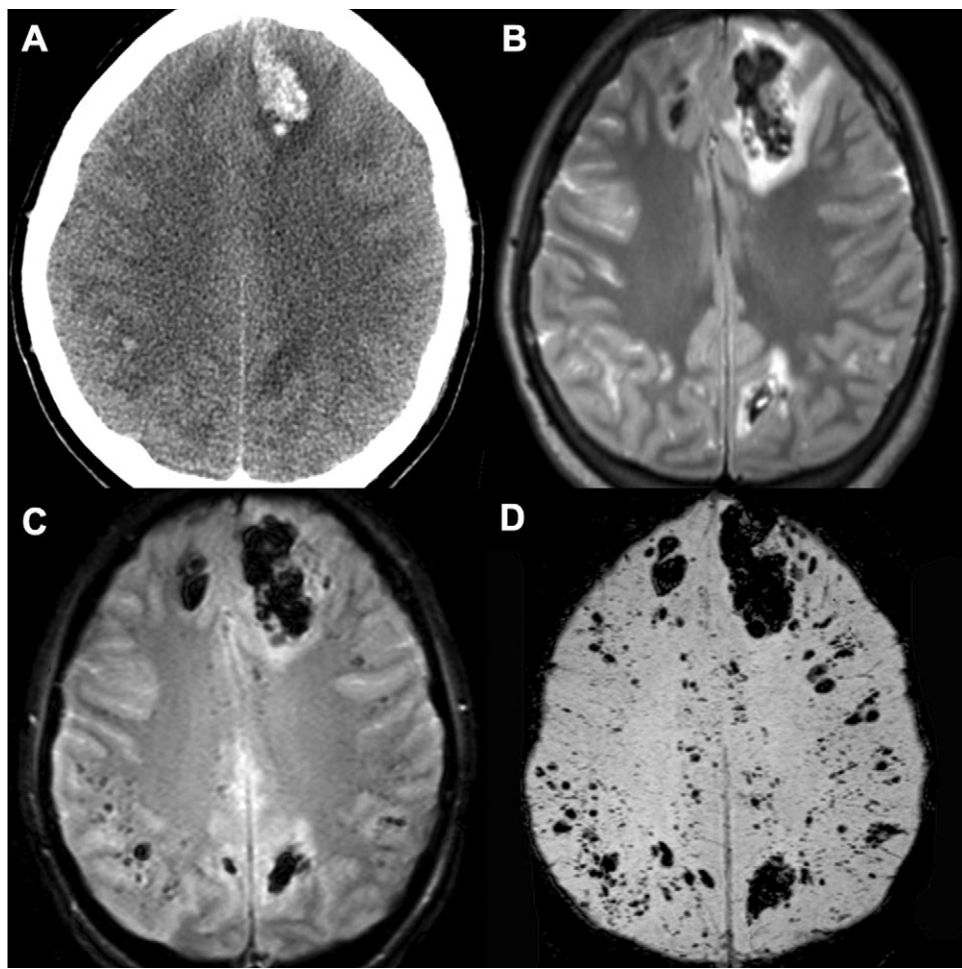


Figure 22: A, Noncontrast-enhanced CT scan of the brain in a young man after motor vehicle crash shows intraparenchymal hemorrhage in the left frontal lobe and smaller hyperdensities in the subcortical regions of the right hemisphere. B, Axial T2-weighted MRI findings confirmed the manifestation of hemorrhages with associated edema. C, D, Susceptibility-weighted imaging shows multiple round and linear hypointensities in both hemispheres representing diffuse vascular injury.

T2-weighted fluid-attenuated inversion recovery images of the pyramidal tract and hypointense signal at susceptibility imaging of the primary motor cortex (Fig 24). However, this imaging finding is not specific to amyotrophic lateral sclerosis and also occurs in less common motor neuron diseases such as primary lateral sclerosis. Again, findings are known from T2*-weighted imaging but more evident at SWI. QSM might become a more objective imaging marker in the future.

Venous Sinus Thrombosis

SWI-like sequences may depict clots in dural sinus thrombosis, notably at early stages a few days after the clinical symptom onset (49). Because there are other established MRI techniques for the depiction of sinus thrombosis, the added value of susceptibility imaging remains moderate. The added value might be more relevant for superficial cortical venous thrombosis. However, the variability of susceptibility imaging between different MRI vendors is considerable. Even within each vendor, there are multiple parameters (eg, flow compensation). Collectively, SWI-like

sequences might provide additional diagnostic clues for superficial vein thrombosis, and suspicious imaging findings should be confirmed by using other MRI sequences. Again, findings are more evident on SWI-like sequences compared with T2* sequences (Fig 25).

Vascular Malformations

Another possible application of susceptibility imaging includes various types of vascular malformations. In arteriovenous malformations, SWI may depict so-called silent intralesional microhemorrhage (50). Moreover, SWI may depict the arterio-venous shunting in brain vascular malformation with a sensitivity of 93%, specificity of 98%, and excellent interobserver agreement of 0.94 (51). The same group (15) used SWI after the injection of gadolinium chelate, whereas SWI normally is performed without contrast material injection. At postcontrast SWI, arteries appear even more hyperintense because of the enhanced time-of-flight effect, whereas veins become hypointense because of an even more pronounced T2* effect. Postcontrast SWI further improved sensitivity to 100% and specificity to 100% to depict the shunt (15).

Table 4: Overview of Key Imaging Findings of Superficial Siderosis in Various Diseases

Parameter	Key Imaging Findings
Trauma	Residual superficial siderosis can occur anywhere, oftentimes of the convexity. Other trauma-related findings such as diffuse axonal injuries or brain contusion may be associated.
CAA	Superficial siderosis has a predilection for parieto-occipital regions. Other imaging findings such as cerebral microbleeds in a peripheral distribution, white matter alterations and lacunes may be associated
Ruptured aneurysm	Clinical history of ruptured aneurysm, subarachnoid hemorrhage in acute stage may develop into superficial siderosis later on
RCVS	Predilection of superficial siderosis at the convexity. Look for associated transient vasoconstriction. Clinical presentation thunderclap headache.
Cryptic vascular malformations (eg, cavernoma)	Superficial siderosis oftentimes most pronounced in posterior fossa of posterior fossa and spinal

Note.—CAA = cerebral amyloid angiopathy, RCVS = reversible cerebral vasoconstriction syndrome.

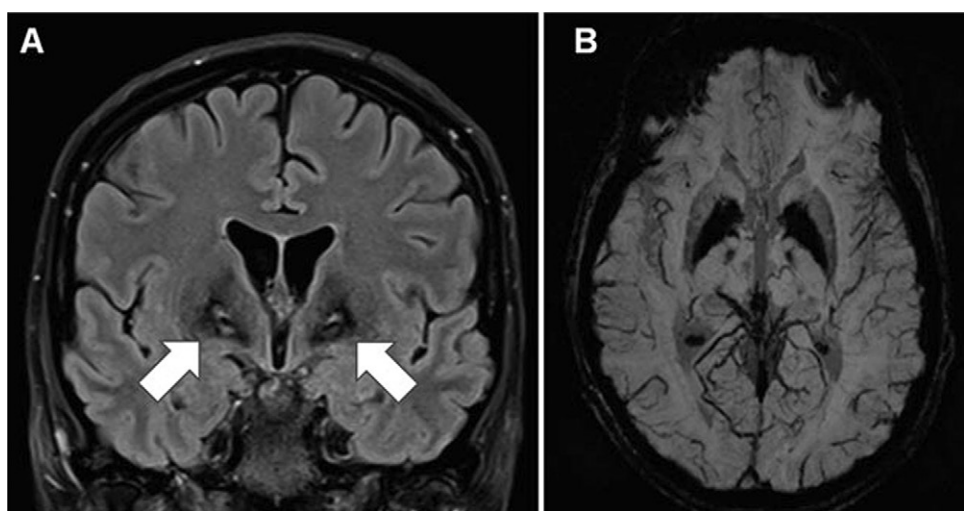


Figure 23: A, Coronal T2-weighted fluid-attenuated inversion recovery image and, B, axial susceptibility-weighted minimum-intensity projection image show typical “eye of the tiger” sign of the pallidum (arrows) in pantothenate kinase-associated neurodegeneration (formerly known as Hallervorden Spatz disease). (Reprinted, with permission, from reference 58.)

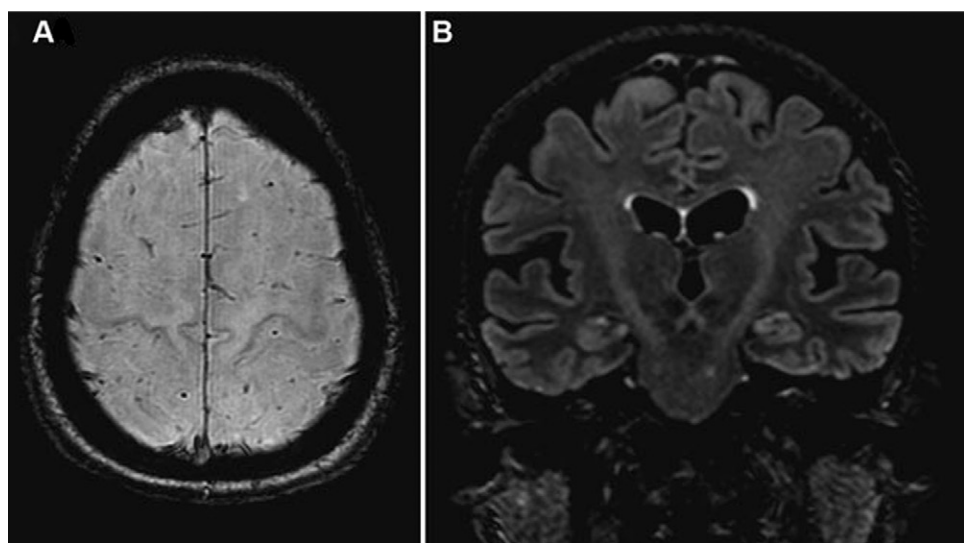


Figure 24: A, Typical hypointense linear signal in the motor cortex area on susceptibility image in amyotrophic lateral sclerosis, associated with hyperintense signal on, B, T2-weighted fluid-attenuated inversion recovery image along the pyramidal tract. Note that those findings are not specific for amyotrophic lateral sclerosis and may occur in primary lateral sclerosis, for example. (Reprinted, with permission, from reference 58.)

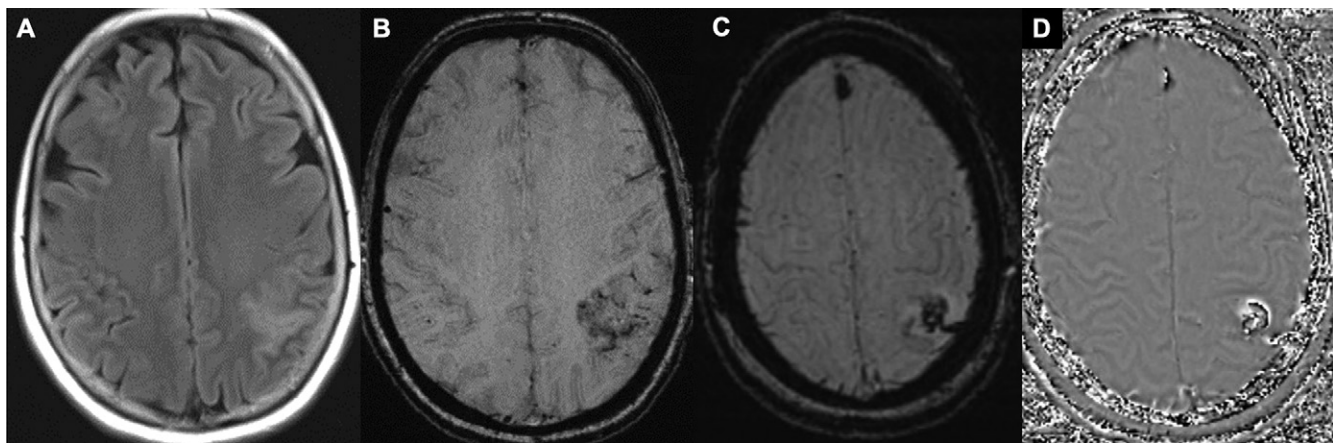


Figure 25: A, Fluid-attenuated inversion recovery image shows hyperintense abnormality in the left parietal region, with petechial hypointensities on, B, susceptibility-weighted image (SWI), representing venous infarction with hemorrhagic component. Cortical vein thrombosis is clearly depicted on images with, C, SWI-like magnitude and, D, phase.

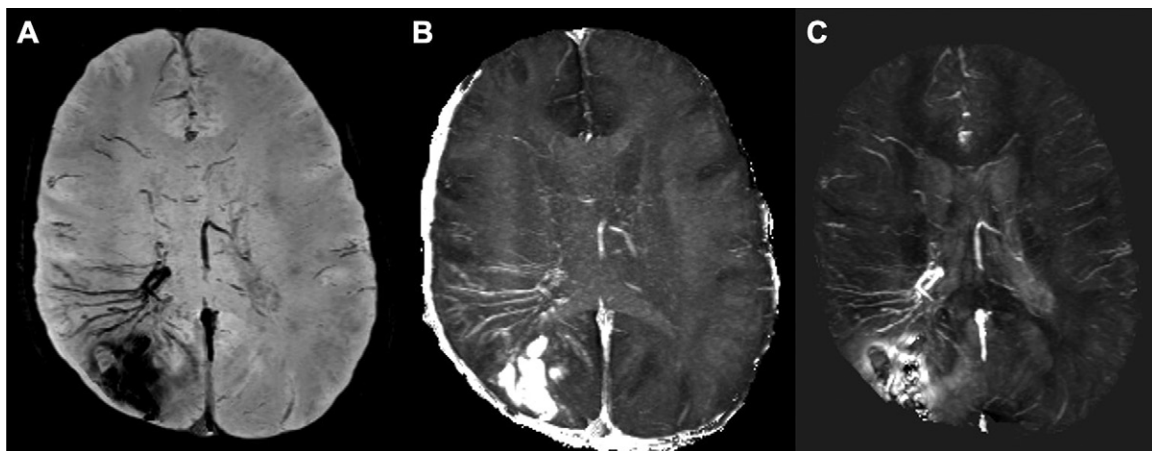


Figure 26: Images in a patient with Sturge-Weber syndrome. A, TrueSWI (trueSWI is postprocessing for the same data set that avoids geometric-induced phase variation by using the source magnetic susceptibility as a mask), B, R2* image, and, C, quantitative susceptibility mapping (QSM) image. Images were minimum intensity projections over eight sections for the trueSWI data and maximum intensity projection over eight sections for the R2* and QSM data (giving an effective section thickness of 16 mm). Acquisition parameters were as follows: repetition time msec/echo time msec, 25/5–17.5; flip angle, 6°; bandwidth, 210 Hz per pixel; acquisition time, 4:58 minutes. (Images courtesy of Csaba Juhasz, Yang Xuan, and Yongsheng Chen, Wayne State University.)

In a similar manner, magnitude images may discriminate different components of vascular malformations and contribute to the detection of the draining vein (52).

Although this is an interesting concept, the technical variability of the various susceptibility sequences across the different MRI vendors is important to consider. Moreover, even within a given MRI sequence or vendor, there may or may not be a variable degree of flow compensation mechanism in the susceptibility sequence. The studies we referenced (15,50–52) used single MRI systems, and it remains to be determined how well those results transfer to other MRI systems.

Vascular Variants

Capillary telangiectasia and developmental venous anomaly.—Capillary telangiectasia is a common incidental finding at brain MRI with typical location in the pons, but it can occur

elsewhere in the brain (Fig E8 [online]). Although it is often isointense on T2-weighted and fluid-attenuated inversion recovery images, these lesions may cause confusion on postcontrast images because of their persistent enhancement. SWI-like sequences can make an important contribution (53) by showing marked susceptibility effects consistent with the histologic finding of dilated venous structures. Developmental venous anomalies are more frequently seen and best seen by using SWI-like sequences (Fig E9 [online]). Sometimes developmental venous anomalies are associated with cavernomas, which are a diagnostic clue if present.

Sturge-Weber syndrome.—Sturge-Weber syndrome is another disease with abnormal veins. Usually, a contrast agent is administered to image children with this disease. But SWI and QSM may serve as a surrogate to the administration of contrast agent, and are possibly more sensitive to the venous,

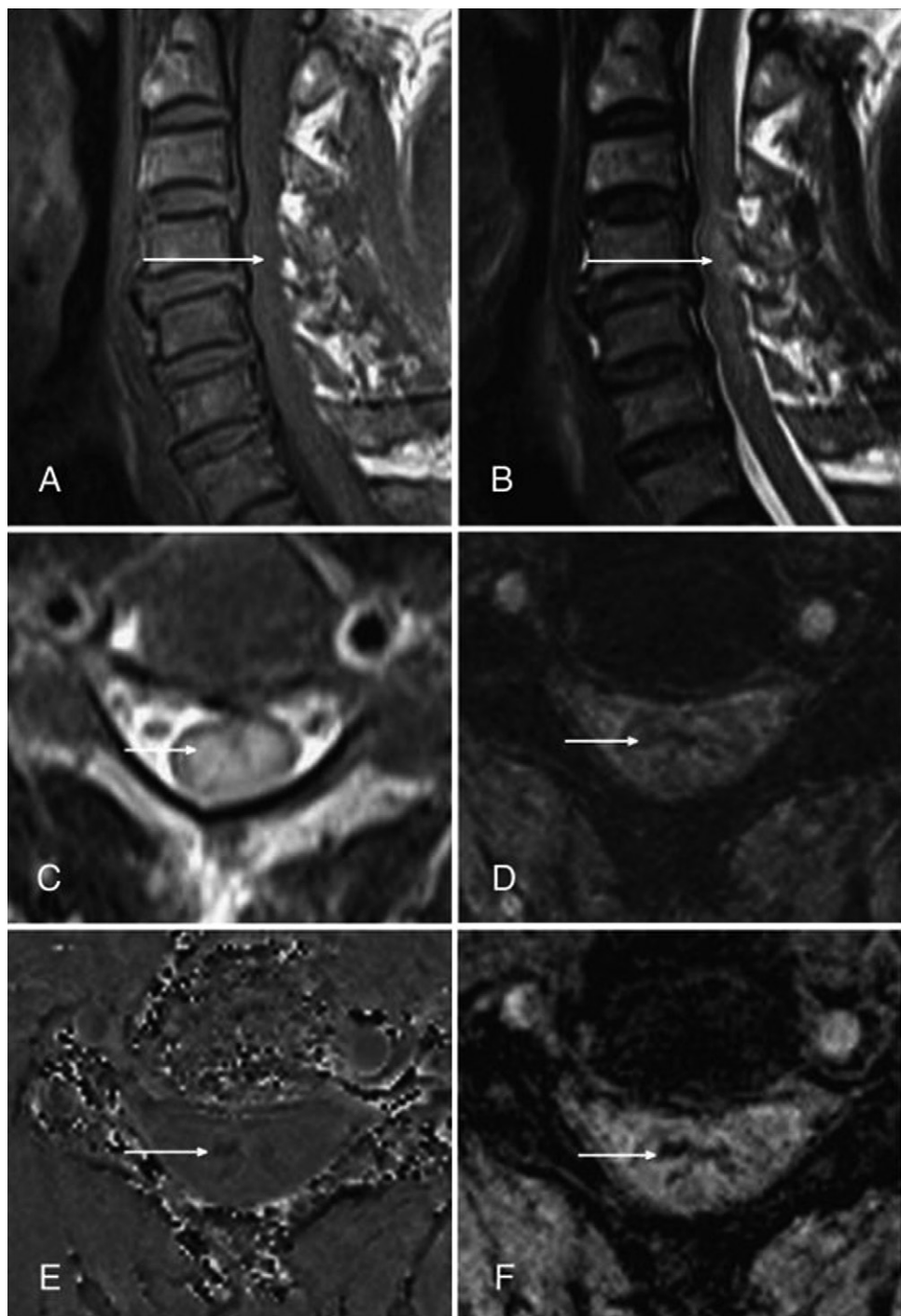


Figure 27: Example of a traumatic cervical spinal cord injury (arrows) on, A, sagittal T1-weighted, B, sagittal T2-weighted, and, C, axial T2-weighted images. Susceptibility-weighted imaging (E, phase; F, magnitude) shows intramedullary hemorrhage more clearly than, D, axial T2*-weighted imaging (D). (Reprinted, with permission, from reference 55.)

oxygen saturation, and calcification elements of the disease. By using high spatial resolution, SWI-like sequences performed in roughly 5 minutes can depict common signs of Sturge-Weber syndrome like impaired cortical veins and abnormal deep venous collaterals (54) (Fig 26).

SWI-like imaging in the spine.—Applications of susceptibility imaging in the spine remain scarce. As a clinically

relevant application, susceptibility imaging can depict post-traumatic intramedullary hemorrhage (55). In a series of 23 patients with acute cervical spine trauma, SWI findings demonstrated additional intramedullary hemorrhage in two of the five patients with spinal contusion at conventional MRI, indicating that susceptibility imaging is more sensitive than conventional MRI in depicting hemorrhage in acute cervical spinal cord injury (Fig 27). However, SWI-

like imaging remains challenging at the level of the spine and notably the cervical spinal cord because of pulsation and respiration artifacts.

SWI-like imaging in children.—Similar to imaging in adults, SWI-like imaging findings provide diagnostic information for a wide range of diseases in children, including neonatal imaging (hemorrhages), metabolic and neurodegenerative diseases (iron deposition and QSM for myelin structure), acute trauma (blood), neoplasm (calcification and blood), and a variety of vascular diseases.

The distribution of intratumoral susceptibility signals in pediatric tumors differs somewhat compared with adults (56).

Conclusion

Susceptibility-weighted imaging (SWI) and SWI-like sequences were initially intended to enhance susceptibility contrast and conspicuity compared with standard gradient-echo T2*-weighted imaging. However, because of the enhanced susceptibility contrast, numerous clinical signs and applications emerged that are specific to high-spatial-resolution, three-dimensional, SWI-like sequences. Because SWI-like image contrast depends entirely on the imaging parameters and its implementation, and because quality can vary between vendors, the reader should be aware of the fundamental technical aspects for a successful data acquisition and image interpretation.

Disclosures of Conflicts of Interest: S.H. Activities related to the present article: disclosed no relevant relationships. Activities not related to the present article: disclosed payment for lectures from GE. Other relationships: disclosed no relevant relationships. E.M.H. Activities related to the present article: disclosed no relevant relationships. Activities not related to the present article: disclosed no relevant relationships. Other relationships: disclosed that author is the chief scientific officer at SpinTech; disclosed SWI patents without active agreements. M.M.T. Activities related to the present article: disclosed no relevant relationships. Activities not related to the present article: disclosed payment for lectures from Biogen; disclosed royalties from Elsevier. Other relationships: disclosed no relevant relationships. F.B. Activities related to the present article: disclosed no relevant relationships. Activities not related to the present article: disclosed payment for board memberships from Biogen, Roche, Merck, Bayer; consultancy with Ixico, Roche, Combinostics; grants from IMI, EU-H2020, BRC, TEVA, and Novartis; payment for lectures from IDKD; royalties from Springer. Other relationships: disclosed no relevant relationships.

References

- Haacke EM, Xu Y, Cheng YC, Reichenbach JR. Susceptibility weighted imaging (SWI). *Magn Reson Med* 2004;52(3):612–618.
- Liu S, Buch S, Chen Y, et al. Susceptibility-weighted imaging: current status and future directions. *NMR Biomed* 2017;30(4):e3552.
- Haacke EM, Liu S, Buch S, Zheng W, Wu D, Ye Y. Quantitative susceptibility mapping: current status and future directions. *Magn Reson Imaging* 2015;33(1):1–25.
- Yamada N, Imakita S, Sakuma T, Takamiya M. Intracranial calcification on gradient-echo phase image: depiction of diamagnetic susceptibility. *Radiology* 1996;198(1):171–178.
- E. MH, Robert WB, Michael RT et al. *Magn Reson Imaging* 1999.
- Reichenbach JR, Venkatesan R, Yablonskiy DA, Thompson MR, Lai S, Haacke EM. Theory and application of static field inhomogeneity effects in gradient-echo imaging. *J Magn Reson Imaging* 1997;7(2):266–279.
- E. MH, & Jürgen RR. Susceptibility Weighted Imaging in MRI. 2014.
- Haacke EM, Lai S, Yablonskiy DA, Lin W. In vivo validation of the bold mechanism: A review of signal changes in gradient echo functional MRI in the presence of flow. *Int J Imaging Syst Technol* 1995;6(2-3):153–163.
- Reichenbach JR, Venkatesan R, Schillinger DJ, Kido DK, Haacke EM. Small vessels in the human brain: MR venography with deoxyhemoglobin as an intrinsic contrast agent. *Radiology* 1997;204(1):272–277.
- Hodel J, Rodallec M, Gerber S, et al. Susceptibility weighted magnetic resonance sequences “SWAN, SWI and VenoBOLD”: technical aspects and clinical applications [in French]. *J Neuroradiol* 2012;39(2):71–86.
- Wu Z, Mittal S, Kish K, Yu Y, Hu J, Haacke EM. Identification of calcification with MRI using susceptibility-weighted imaging: a case study. *J Magn Reson Imaging* 2009;29(1):177–182.
- Xu Y, Haacke EM. The role of voxel aspect ratio in determining apparent vascular phase behavior in susceptibility weighted imaging. *Magn Reson Imaging* 2006;24(2):155–160.
- Wu D, Liu S, Buch S, Ye Y, Dai Y, Haacke EM. A fully flow-compensated multiecho susceptibility-weighted imaging sequence: The effects of acceleration and background field on flow compensation. *Magn Reson Med* 2016;76(2):478–489.
- Liu S, Mok K, Neelavalli J, et al. Improved MR venography using quantitative susceptibility-weighted imaging. *J Magn Reson Imaging* 2014;40(3):698–708.
- Jagadeesan BD, Delgado Almandoz JE, Benzinger TL, Moran CJ. Postcontrast susceptibility-weighted imaging: a novel technique for the detection of arteriovenous shunting in vascular malformations of the brain. *Stroke* 2011;42(11):3127–3131.
- Li W, Liu C, Duong TQ, van Zijl PC, Li X. Susceptibility tensor imaging (STI) of the brain. *NMR Biomed* 2017;30(4):e3540.
- Nandigam RN, Viswanathan A, Delgado P, et al. MR imaging detection of cerebral microbleeds: effect of susceptibility-weighted imaging, section thickness, and field strength. *AJR Am J Neuroradiol* 2009;30(2):338–343.
- Schwarz ST, Afzal M, Morgan PS, Bajaj N, Gowland PA, Auer DP. The ‘swallow tail’ appearance of the healthy nigrosome - a new accurate test of Parkinson’s disease: a case-control and retrospective cross-sectional MRI study at 3T. *PLoS One* 2014;9(4):e93814.
- Azuma M, Hirai T, Yamada K, et al. Lateral Asymmetry and Spatial Difference of Iron Deposition in the Substantia Nigra of Patients with Parkinson Disease Measured with Quantitative Susceptibility Mapping. *AJR Am J Neuroradiol* 2016;37(5):782–788.
- Meijer FJ, Steens SC, van Rumund A, et al. Nigrosome-1 on Susceptibility Weighted Imaging to Differentiate Parkinson’s Disease From Atypical Parkinsonism: An In Vivo and Ex Vivo Pilot Study. *Pol J Radiol* 2016;81:363–369.
- Perez Akly MS, Stefani CV, Ciancaglini L, et al. Accuracy of nigrosome-1 detection to discriminate patients with Parkinson’s disease and essential tremor. *Neuroradiol J* 2019;32(6):395–400.
- Sung YH, Noh Y, Lee J, Kim EY. Drug-induced Parkinsonism versus Idiopathic Parkinson Disease: Utility of Nigrosome 1 with 3-T Imaging. *Radiology* 2016;279(3):849–858.
- Haller S, Fällmar D, Larsson EM. Susceptibility weighted imaging in dementia with Lewy bodies: will it resolve the blind spot of MRI? *Neuroradiology* 2016;58(2):217–218.
- Shams S, Fällmar D, Schwarz S, et al. MRI of the Swallow Tail Sign: A Useful Marker in the Diagnosis of Lewy Body Dementia? *AJR Am J Neuroradiol* 2017;38(9):1737–1741.
- Kamagata K, Nakatsuka T, Sakakibara R, et al. Diagnostic imaging of dementia with Lewy bodies by susceptibility-weighted imaging of nigrosomes versus striatal dopamine transporter single-photon emission computed tomography: a retrospective observational study. *Neuroradiology* 2017;59(1):89–98 [Published correction appears in *Neuroradiology* 2017;59(4):425.]
- Cheng Z, He N, Huang P, et al. Imaging the Nigrosome 1 in the substantia nigra using susceptibility weighted imaging and quantitative susceptibility mapping: An application to Parkinson’s disease. *Neuroimage Clin* 2020;25:102103.
- Thompson AJ, Banwell BL, Barkhof F, et al. Diagnosis of multiple sclerosis: 2017 revisions of the McDonald criteria. *Lancet Neurol* 2018;17(2):162–173.
- Sparacia G, Agnello F, Gambino A, Sciortino M, Midiri M. Multiple sclerosis: High prevalence of the ‘central vein’ sign in white matter lesions on susceptibility-weighted images. *Neuroradiol J* 2018;31(4):356–361.
- Absinta M, Sati P, Masuzzo F, et al. Association of Chronic Active Multiple Sclerosis Lesions With Disability In Vivo. *JAMA Neurol* 2019;76(12):1474–1483.
- Sati P, George IC, Shea CD, Gaitán MI, Reich DS. FLAIR*: a combined MR contrast technique for visualizing white matter lesions and parenchymal veins. *Radiology* 2012;265(3):926–932.
- Thurnher MM, Boban J, Rieger A, Gelpi E. Susceptibility-Weighted MR Imaging Hypointense Rim in Progressive Multifocal Leukoencephalopathy: The End Point of Neuroinflammation and a Potential Outcome Predictor. *AJR Am J Neuroradiol* 2019;40(6):994–1000.
- Riedel CH, Zimmermann P, Jensen-Kondering U, Stengele R, Deuschl G, Jansen O. The importance of size: successful recanalization by intravenous thrombolysis in acute anterior stroke depends on thrombus length. *Stroke* 2011;42(6):1775–1777.

33. Weisstanner C, Gratz PP, Schroth G, et al. Thrombus imaging in acute stroke: correlation of thrombus length on susceptibility-weighted imaging with endovascular reperfusion success. *Eur Radiol* 2014;24(8):1735–1741.
34. Xia S, Utriainen D, Tang J, et al. Decreased oxygen saturation in asymmetrically prominent cortical veins in patients with cerebral ischemic stroke. *Magn Reson Imaging* 2014;32(10):1272–1276.
35. Dejobert M, Cazals X, Annan M, Debiais S, Lauvin MA, Cottier JP. Susceptibility-Diffusion Mismatch in Hyperacute Stroke: Correlation with Perfusion-Diffusion Mismatch and Clinical Outcome. *J Stroke Cerebrovasc Dis* 2016;25(7):1760–1766.
36. Liu H, Mei W, Li Y, et al. Susceptibility-diffusion mismatch: an effective method by which to detect perfusion-diffusion mismatch in acute ischemic stroke. *Int J Clin Exp Med* 2016;9(10):19691–19699.
37. Wang Y, Shi T, Chen B, Lin G, Xu Y, Geng Y. Prominent hypointense vessel sign on susceptibility-weighted imaging is associated with clinical outcome in acute ischaemic stroke. *Eur Neurol* 2018;79(5-6):231–239.
38. Radbruch A, Wiestler B, Kramp L, et al. Differentiation of glioblastoma and primary CNS lymphomas using susceptibility weighted imaging. *Eur J Radiol* 2013;82(3):552–556.
39. Saini J, Gupta PK, Sahoo P, et al. Differentiation of grade II/III and grade IV glioma by combining “T1 contrast-enhanced brain perfusion imaging” and susceptibility-weighted quantitative imaging. *Neuroradiology* 2018;60(1):43–50.
40. Park MJ, Kim HS, Jahng GH, Ryu CW, Park SM, Kim SY. Semiquantitative assessment of intratumoral susceptibility signals using non-contrast-enhanced high-field high-resolution susceptibility-weighted imaging in patients with gliomas: comparison with MR perfusion imaging. *AJNR Am J Neuroradiol* 2009;30(7):1402–1408.
41. Toh CH, Wei KC, Chang CN, et al. Differentiation of pyogenic brain abscesses from necrotic glioblastomas with use of susceptibility-weighted imaging. *AJNR Am J Neuroradiol* 2012;33(8):1534–1538.
42. Antulov R, Dolic K, Fruehwald-Pallamar J, Miletic D, Thurnher MM. Differentiation of pyogenic and fungal brain abscesses with susceptibility-weighted MR sequences. *Neuroradiology* 2014;56(11):937–945.
43. Haller S, Vernooy MW, Kuijer JPA, Larsson EM, Jäger HR, Barkhof F. Cerebral Microbleeds: Imaging and Clinical Significance. *Radiology* 2018;287(1):11–28.
44. Beauchamp MH, Ditchfield M, Babl FE, et al. Detecting traumatic brain lesions in children: CT versus MRI versus susceptibility weighted imaging (SWI). *J Neurotrauma* 2011;28(6):915–927.
45. Haller S. The Concept of “Number Needed to Image”. *AJNRAm J Neuroradiol* 2017;38(10):E79–E80.
46. Liu W, Soderlund K, Senseney JS, et al. Imaging Cerebral Microhemorrhages in Military Service Members with Chronic Traumatic Brain Injury. *Radiology* 2016;278(2):536–545.
47. Iwamura A, Taoka T, Fukusumi A, et al. Diffuse vascular injury: convergent-type hemorrhage in the supratentorial white matter on susceptibility-weighted image in cases of severe traumatic brain damage. *Neuroradiology* 2012;54(4):335–343.
48. Kruer MC, Boddaert N, Schneider SA, et al. Neuroimaging features of neurodegeneration with brain iron accumulation. *AJNR Am J Neuroradiol* 2012;33(3):407–414.
49. Idibaih A, Boukobza M, Crassard I, Porcher R, Bousser MG, Chabriat H. MRI of clot in cerebral venous thrombosis: high diagnostic value of susceptibility-weighted images. *Stroke* 2006;37(4):991–995.
50. Guo Y, Saunders T, Su H, et al. Silent intralosomal microhemorrhage as a risk factor for brain arteriovenous malformation rupture. *Stroke* 2012;43(5):1240–1246.
51. Jagadeesan BD, Delgado Almandoz JE, Moran CJ, Benzinger TL. Accuracy of susceptibility-weighted imaging for the detection of arteriovenous shunting in vascular malformations of the brain. *Stroke* 2011;42(1):87–92.
52. Miyasaka T, Taoka T, Nakagawa H, et al. Application of susceptibility weighted imaging (SWI) for evaluation of draining veins of arteriovenous malformation: utility of magnitude images. *Neuroradiology* 2012;54(11):1221–1227.
53. El-Koussy M, Schroth G, Gralla J, et al. Susceptibility-weighted MR imaging for diagnosis of capillary telangiectasia of the brain. *AJNR Am J Neuroradiol* 2012;33(4):715–720.
54. Hu J, Yu Y, Juhasz C, et al. MR susceptibility weighted imaging (SWI) complements conventional contrast enhanced T1 weighted MRI in characterizing brain abnormalities of Sturge-Weber Syndrome. *J Magn Reson Imaging* 2008;28(2):300–307.
55. Wang M, Dai Y, Han Y, Haacke EM, Dai J, Shi D. Susceptibility weighted imaging in detecting hemorrhage in acute cervical spinal cord injury. *Magn Reson Imaging* 2011;29(3):365–373.
56. Gaudino S, Marziali G, Pezzullo G, et al. Role of susceptibility-weighted imaging and intratumoral susceptibility signals in grading and differentiating pediatric brain tumors at 1.5 T: a preliminary study. *Neuroradiology* 2020;62(6):705–713.
57. Soman S, Holdsworth SJ, Barnes PD, et al. Improved T2* imaging without increase in scan time: SWI processing of 2D gradient echo. *AJNR Am J Neuroradiol* 2013;34(11):2092–2097.
58. Haller S, Garibotto V, Schwarz S. Neuroimaging in Movement Disorders. In: Barkhof F, Jager R, Thurnher M, et al, eds. *Clinical Neuroradiology*. Cham, Switzerland: Springer, 2018; 1–36.